COMMUN. MATH. SCI.
Vol. 10, No. 1, pp. 355–385

SIMULATION OF FLUID–PARTICLES FLOWS: HEAVY PARTICLES, FLOWING REGIME, AND ASYMPTOTIC-PRESERVING SCHEMES*

THIERRY GOUDON†, SHI JIN‡, AND BOKAI YAN§

To Dave Levermore on his 60th birthday with friendship and appreciation

Abstract. We are interested in an Eulerian–Lagrangian model describing particulate flows. The model under study consists of the Euler system and a Vlasov-Fokker-Planck equation coupled through momentum and energy exchanges. This problem contains asymptotic regimes that make the coupling terms stiff, and lead to a limiting model of purely hydrodynamic type. We design a numerical scheme which is able to capture this asymptotic behavior without requiring prohibitive stability conditions. The construction of this Asymptotic Preserving scheme relies on an implicit discretization of the stiff terms which can be treated by efficient inversion methods. This method is a natural coupling of a kinetic solver for the particles with a kinetic scheme for the hydrodynamic Euler equations. Numerical experiments are conducted to study the performance of this scheme in various asymptotic regimes.

Key words. Fluid–particles flows, hydrodynamic regimes, Asymptotic Preserving schemes, Kinetic schemes.

AMS subject classifications. 82C80, 82C40, 35L65, 35Q35, 65M06, 76N15, 76M20.

1. Introduction

This paper is devoted to the numerical simulation of certain two-phase flows, where a disperse phase, which is a large set of "particles" that could be bubbles, droplets, dusts, etc. interacts with a dense phase — the surrounding fluid. There are many possible models for such flows. The microscopic models are based on fluid equations defined on disjoint domains and coupled by time-varying interface boundary conditions. The macroscopic (or "Eulerian–Eulerian") models are based on coupled fluid equations describing both phases and defined on a common domain, and these models involve volume fraction and non-conservative terms [30]. The mesoscopic models consist of coupled fluid and kinetic equations. We refer for instance to the overview [19] for a presentation of the different approaches. In what follows we are concerned with the so-called "Eulerian-Lagrangian" framework, or "mesoscopic" description where we adopt a statistical viewpoint for the disperse phase. It means that the set of particles is described through a particle distribution function $f(t,x,v)$ in phase space; the integral

$$\int_\Omega f(t,x,v)\,\mathrm{d}v\,\mathrm{d}x$$

*Received: February 3, 2011; accepted (in revised version): August 8, 2011. This work was partially supported by NSF grant No. DMS-0608720 and NSF FRG grant DMS-0757285. SJ was also supported by a Van Vleck Distinguished Research Prize and a Vilas Associate Award from University of Wisconsin-Madison.

†Project-Team SIMPAF, INRIA Lille Nord Europe Research Centre, Park Plazza, 40 avenue Halley, 59650 Villeneuve d'Ascq cedex, France and Labo P. Painlevé UMR 8524 CNRS & Université des Sciences et Technologies Lille 1, France (thierry.goudon@inria.fr).

‡Department of Mathematics, University of Wisconsin–Madison, 480 Lincoln Drive, Madison, WI 53706, USA (jin@math.wisc.edu).

§Department of Mathematics, University of Wisconsin–Madison, 480 Lincoln Drive, Madison, WI 53706, USA (yan@math.wisc.edu).

represents the number of particles occupying at time t the volume $\Omega \subset \mathbb{R}^N \times \mathbb{R}^N$ of the phase space, x being the position variable and v the velocity variable. The particle distribution function can be associated with the macroscopic quantities — those observable by experiments — by taking the moments:

$$\begin{cases} \text{the macroscopic density:} & n(t,x) = \displaystyle\int_{\mathbb{R}^N} f(t,x,v)\,\mathrm{d}v, \\ \text{the momentum:} & nV(t,x) = \displaystyle\int_{\mathbb{R}^N} v\ f(t,x,v)\,\mathrm{d}v, \\ \text{the total energy:} & E_P(t,x) = \dfrac{n}{2}|V|^2 + \dfrac{1}{2}Nn\Theta_P = \displaystyle\int_{\mathbb{R}^N} \frac{|v|^2}{2}\ f(t,x,v)\,\mathrm{d}v, \\ \text{the heat flux:} & q(t,x) = \displaystyle\int_{\mathbb{R}^N} v\ \frac{|v|^2}{2}\ f(t,x,v)\,\mathrm{d}v. \end{cases}$$

Here V is the averaged particle velocity, and Θ_P the temperature of particles. The fluid is described by its density $\rho(t,x) \geq 0$, its velocity $u(t,x) \in \mathbb{R}^N$, and its total energy $E(t,x) \geq 0$. For further purposes, we introduce the internal energy e, the pressure p, and the temperature Θ defined by the relations

$$e = \frac{p}{(\gamma-1)\rho} \geq 0, \qquad p = \rho\Theta, \qquad E = e + \frac{u^2}{2},$$

where $1 < \gamma \leq (N+2)/N$ is the adiabatic constant.

According to the hierarchy introduced by O'Rourke [42], we are interested in the so–called "Thin Sprays" where the two phases interact through momentum and energy exchanges, but the effect due to the volume fraction of the particles is neglected. The leading effect that couples the evolution of the disperse and dense phases is due to drag forces. In the system of PDEs we need to introduce a few more physical quantities:

- $\rho_P > 0$ and $\rho_F > 0$ stand for the typical mass densities of the particles and of the fluid, respectively.
- Both phases are subject to an external potential Φ which deviates the trajectories of the particles. The (real–valued) coefficients η_F and η_P account for the fact that the external potential can act differently, both in orientation and amplitude, on the two phases. A typical example is given by gravity/buoyancy forces. In this case $\nabla_x \Phi = g e_z$, with e_z the unit downward vector, g is the gravitational acceleration, and we set $\eta_F = 1$, $\eta_P = (1 - \rho_F/\rho_P)$. Other relevant examples are given by centrifugal forces or electric forces when considering charged particles immersed in a neutral fluid.
- The Stokes number $\varepsilon > 0$ is the ratio of the Stokes settling time (that is $\frac{2\rho_F a^2}{9\mu}$, with μ the dynamic viscosity of the fluid and a the typical radius of the particles) over a certain time unit of observation. It characterizes the strength of the drag exerted by the fluid on the particles.

We shall work on a simplified dimensionless version of the equations which govern the system, reducing the number of physical parameters and focusing on the role of the scaling parameter ε. The discussion of the scaling issues is detailed in the Appendix, and we refer to [5, 7, 12, 13, 38] for thorough comments. On the one hand, the evolution of the density f is determined by the Fokker-Planck equation

$$\partial_t f + v \cdot \nabla_x f = \frac{1}{\varepsilon} L_{u,\Theta} f + \eta_P \nabla_x \Phi \cdot \nabla_v f, \tag{1.1}$$

where

$$L_{u,\Theta} f = \mathrm{Div}_v\big((v-u)f + \Theta \nabla_v f\big). \tag{1.2}$$

On the other hand, the evolution of the fluid obeys the Euler system

$$\begin{cases} \partial_t \rho + \mathrm{Div}_x(\rho u) = 0, \\ \partial_t(\rho u) + \mathrm{Div}_x(\rho u \otimes u) + \nabla_x p = \dfrac{1}{\varepsilon}\dfrac{\rho_P}{\rho_F}\mathscr{F} - \eta_F \rho \nabla_x \Phi, \\ \partial_t(\rho E) + \mathrm{Div}_x\big((\rho E + p)u\big) = \dfrac{1}{\varepsilon}\dfrac{\rho_P}{\rho_F}\mathscr{E} - \eta_F \rho u \cdot \nabla_x \Phi. \end{cases} \tag{1.3}$$

The Fokker-Planck operator $L_{u,\Theta}$ in (1.2) describes the following physical effects the particles are subject to due to their environment:

- The drag force exerted by the surrounding fluid is supposed to be proportional to the relative velocity $(v-u)$;
- Diffusion with respect to the velocity variable arises due to the Brownian motion, which involves the temperature Θ of the fluid [20, 21].

Many additional effects are simply disregarded, such as the added mass effect, the interparticles collisions, or size variations due to coagulation and break–up phenomena. Note that the viscosity of the fluid enters in the definition of the parameter ε while viscous effects are neglected on the evolution of the fluid. This can be justified, at least formally, by suitable scaling arguments. The disperse phase influences the dense phase through the coupling terms $\mathscr{F}$ and $\mathscr{E}$, which are defined by

$$\begin{aligned} &\text{Momentum Exchanges:} \quad \mathscr{F} = -\int_{\mathbb{R}^N} v\, L_{u,\Theta} f \,\mathrm{d}v = \int_{\mathbb{R}^N} (v-u) f \,\mathrm{d}v = n(V-u), \\ &\text{Energy Exchanges:} \quad \mathscr{E} = -\int_{\mathbb{R}^N} \frac{v^2}{2}\, L_{u,\Theta} f \,\mathrm{d}v = \int_{\mathbb{R}^N} (v(v-u) - N\Theta) f \,\mathrm{d}v \\ &\qquad\qquad = n(V-u)\cdot u + Nn(\Theta_P - \Theta) + n|V-u|^2 \\ &\qquad\qquad = n(V-u)\cdot V + Nn(\Theta_P - \Theta). \end{aligned} \tag{1.4}$$

The definition of the coupling terms $\mathscr{F}$ and $\mathscr{E}$ induces conservation properties. Let us write the system satisfied by the moments of f, that is

$$\begin{aligned} \partial_t n + \mathrm{Div}_x(nV) &= 0, \\ \partial_t(nV) + \mathrm{Div}_x \mathbb{P} + \eta_P n \nabla_x \Phi &= -\frac{1}{\varepsilon} n(V-u), \\ \partial_t \Upsilon + \mathrm{Div}_x q + \eta_P nV \cdot \nabla_x \Phi &= -\frac{n}{\varepsilon}\big((V-u)\cdot V + N(\Theta_P - \Theta)\big) \\ &= -\frac{1}{\varepsilon}(2\Upsilon - nV\cdot u - Nn\Theta), \end{aligned}$$

with $\Upsilon = (nV^2 + Nn\Theta_P)/2$ and $\mathbb{P} = \int_{\mathbb{R}^N} v \otimes v f \,\mathrm{d}v$. Combined with the fluid equations, this leads to the following conservation laws:

$$\begin{aligned} &\partial_t\Big(\rho u + \frac{\rho_P}{\rho_F} nV\Big) + \mathrm{Div}\Big(\rho u \otimes u + p + \frac{\rho_P}{\rho_F}\mathbb{P}\Big) + \Big(\eta_F \rho + \eta_P \frac{\rho_P}{\rho_F} n\Big)\nabla_x \Phi = 0, \\ &\partial_t\Big(\rho E + \frac{\rho_P}{\rho_F}\Upsilon\Big) + \mathrm{Div}\Big((\rho E + p)u + \frac{\rho_P}{\rho_F} q\Big) + \Big(\eta_F \rho u + \eta_P \frac{\rho_P}{\rho_F} nV\Big)\cdot \nabla_x \Phi = 0. \end{aligned} \tag{1.5}$$

The total momentum and the total energy are conserved.

Besides the conservation of total momentum and energy, another key feature of the model is the dissipation property that we describe now. To this end, we introduce the "local Maxwellian":

$$M_{u,\Theta}(v) := (2\pi\Theta)^{-N/2} \exp\Big(-\frac{|v-u|^2}{2\Theta}\Big).$$

The crucial observation consists in rewriting

$$L_{u,\Theta} f = \Theta \ \mathrm{Div}_v\Big(M_{u,\Theta}\nabla_v\Big(\frac{f}{M_{u,\Theta}}\Big)\Big).$$

We consider the fluid–entropy $S(t,x)$ defined by the relation

$$S := -\frac{1}{\gamma-1}\ln\big(p\rho^{-\gamma}\big) = -\frac{1}{\gamma-1}\ln\Big(\frac{\Theta}{\rho^{\gamma-1}}\Big).$$

Then, as already remarked in [5], the total energy is conserved and the total entropy is dissipated since

$$\frac{\mathrm{d}}{\mathrm{d}t}\Big(\rho_{_F}\int_{\mathbb{R}^N}\rho\big(E+\eta_{_F}\Phi\big)\,\mathrm{d}x+\rho_{_P}\int_{\mathbb{R}^N}\int_{\mathbb{R}^N}\Big(\frac{v^2}{2}+\eta_{_P}\Phi\Big)f\,\mathrm{d}v\,\mathrm{d}x\Big)=0 \tag{1.6}$$

and

$$\begin{aligned}&\frac{\mathrm{d}}{\mathrm{d}t}\Big(\rho_{_F}\int_{\mathbb{R}^N}\rho S\,\mathrm{d}x+\rho_{_P}\int_{\mathbb{R}^N}\int_{\mathbb{R}^N} f\ln(f)\,\mathrm{d}v\,\mathrm{d}x\Big)\\ &=-\frac{\rho_{_P}}{\varepsilon}\left(\int_{\mathbb{R}^N}\int_{\mathbb{R}^N}\Big|\sqrt{\Theta}\frac{\nabla_v f}{\sqrt{f}}+\frac{v-V}{\sqrt{\Theta}}\sqrt{f}\Big|^2\,\mathrm{d}v\,\mathrm{d}x+\int_{\mathbb{R}^N}\int_{\mathbb{R}^N} f\frac{|V-u|^2}{\Theta}\,\mathrm{d}v\,\mathrm{d}x\right)\\ &\le 0.\end{aligned} \tag{1.7}$$

Here the problem is defined in the whole space, but similar manipulations hold when considering standard reflection laws for the particles and boundary conditions for the fluid; see [12]. Note that the dissipation terms in (1.7) vanish when

$$u=V \quad \text{and} \quad f(t,x,v)=\frac{n(t,x)}{\big(2\pi\Theta(t,x)\big)^{N/2}}\ \exp\Big(-\frac{|v-V(t,x)|^2}{2\Theta(t,x)}\Big).$$

For such an equilibrium, the temperatures of the two phases equilibrate, $\Theta=\Theta_P$, and they have a common macroscopic velocity.

We are interested in the situation where the parameter ε can become small. In this regime, the conservation and dissipation properties detailed above are the basis to describe the asymptotic behavior of the model. In the next Section we shall formally describe the asymptotic behavior of the solutions for $\varepsilon \ll 1$. In this regime, the operator $L_{u,\Theta}$ and the coupling terms are stiff, and one can expect the relaxation effect that prescribes the form of the particle distribution function, and as a consequence one arrives at a set of macroscopic equations to describe the particles–fluid mixture. In Section 3 we design a numerical scheme able to treat the stiffness of the problem efficiently. This scheme belongs to the class of the so-called Asymptotic-Preserving (AP) schemes because it is able to capture the correct asymptotic behavior without suffering the prohibitive scaling-parameter-dependent numerical constraints; see [31] and for recent overviews [24, 32]. In order to define a scheme for the coupled system we find it convenient to discretize the Euler equations by using the Kinetic schemes [15, 16, 17, 44, 45, 46]. We finally conduct numerical simulations in Section 4, and numerically study some relevant variations of the model.

2. The hydrodynamic regimes

For Equation (1.1), as $\varepsilon \to 0$, the Fokker-Planck operator vanishes, which yields

$$f(t,x,v) \simeq \frac{n(t,x)}{(2\pi\Theta)^{N/2}} \exp\Big(- \frac{|v-u(t,x)|^2}{2\Theta(t,x)} \Big). \tag{2.1}$$

This ansatz is in agreement with the dissipation estimate (1.7). One can now find the limiting equations satisfied by ρ, u, Θ, and n. To this end we go back to the conservation laws (1.5). The ansatz (2.1) yields $nV \simeq nu$, $\Theta_P \simeq \Theta$, $\mathbb{P} \simeq nu \otimes u + n\Theta\mathbb{I}$, and $q \simeq (nu^2 + (N+2)n\Theta)/2$. Therefore one arrives at the following limit system:

$$\begin{aligned}
\partial_t \rho + \mathrm{Div}_x(\rho u) &= 0, \\
\partial_t n + \mathrm{Div}_x(nu) &= 0, \\
\partial_t \Big(\Big(\rho + \frac{\rho_P}{\rho_F} n \Big) u \Big) + \mathrm{Div}_x \Big(\Big(\rho + \frac{\rho_P}{\rho_F} n \Big) u \otimes u + p + \frac{\rho_P}{\rho_F} n\Theta \Big) + \Big(\eta_F \rho + \eta_P \frac{\rho_P}{\rho_F} n \Big) \nabla_x \Phi &= 0, \\
\partial_t \Big(\Big(\rho + \frac{\rho_P}{\rho_F} n \Big) \frac{u^2}{2} + \frac{\rho\Theta}{\gamma - 1} + \frac{\rho_P}{\rho_F} \frac{N}{2} n\Theta \Big) & \\
+ \mathrm{Div}_x \Big(\Big[\Big(\rho + \frac{\rho_P}{\rho_F} n \Big) \frac{u^2}{2} + \frac{\gamma}{\gamma - 1} \rho\Theta + \frac{\rho_P}{\rho_F} \frac{N+2}{2} n\Theta \Big] u \Big) + \Big(\eta_F \rho + \eta_P \frac{\rho_P}{\rho_F} n \Big) u \cdot \nabla_x \Phi &= 0.
\end{aligned} \tag{2.2}$$

The system can be seen as the Euler system for the composite density $\rho + \frac{\rho_P}{\rho_F} n$, the composite pressure $\big(\frac{\gamma}{\gamma-1} \rho + \frac{N+2}{2} \frac{\rho_P}{\rho_F} n \big) \Theta$, the common velocity u, and temperature Θ, plus an additional mass conservation equation for ρ (or n).

The mathematical analysis of such fluid–kinetic systems is highly challenging. The difficulty lies on the nonlinear coupling of PDEs of different nature. Different models for the fluid (compressible or incompressible, viscous or inviscid, etc.) introduce different levels of difficulty. A first attempt was to prove the local existence of smooth solutions; see [3, 38] for the analysis of the Euler-Vlasov systems. Another approach concerning classical solutions restricts to solutions close to the equilibrium by using perturbation techniques and energy estimates [28, 11]. The global existence of weak solutions has been investigated, mainly considering viscous flows, by using fixed point and/or compactness arguments. A crucial step of these proofs relies on the construction of suitable approximations preserving the dissipation properties of the system [29, 39, 40, 6]. Identification of relevant scaling and discussion of asymptotic problems appeared in [10, 26, 27, 40, 12, 5, 38]; see also [14] for the analysis of fine properties of the limit hydrodynamic systems. These problems are motivated by combustion theory [42, 53] with applications for the design of performing engines [22] or rocket propulsors [36]. The equations also arise in the modeling of atmospheric pollution [50, 52], sedimentation processes [4, 8], rain formation [23], or dispersion of volcanic columns [43]. It is also worth mentioning the applications in the description of biomedical sprays [2, 41]. In what follows, we are concerned with the design of an efficient numerical scheme which is specifically suitable for the asymptotic regime of small ε's in (1.1)–(1.3).

3. An AP scheme for the flowing regime

A standard numerical scheme for the system (1.1)–(1.3) faces some difficulties, and becomes inefficient in the regime $0 < \varepsilon \ll 1$. The main numerical issues include:

a) The presence of stiff terms leads to the increase of computational cost due to numerical stability constraints;

b) The scheme is required to recover, as ε goes to 0, the behavior of the solutions of the limit Equations (2.2) with ε-independent mesh sizes and time steps;

c) The system couples kinetic and hydrodynamic equations;

d) The system has remarkable conservation and dissipation properties that, ideally, should be preserved at the discrete level.

These questions were already addressed in [13], for isentropic flows, where splitting methods are introduced: the kinetic equation is solved first, the hydrodynamic fields being fixed during this time step; then, (ρ,u,Θ) are updated by using an anti-diffusive scheme for the Euler system (see [18, 34, 35]) with source terms defined using the new values of the particle distribution function. This strategy is very efficient when dealing with another scaling — the so-called "Bubbling Regime" — of the equation which yields a diffusion equation for the particle density; see also [7] for the discussion of energy exchanges. In [13] the splitting method has been adapted to the present scaling. Here we propose a different approach to treat the Flowing Regime: the method we propose combines the AP approach and kinetic schemes for the hydrodynamic equations. It contains a very efficient implementation of the implicit stiff terms, and with the desired AP properties in the small ε regimes.

3.1. The time discretization – first order. First, the stiff source terms will be discretized implicitly in order to allow ε-independent time steps. Let $\Delta t>0$ be the time step, and U^k denote the numerical approximation of a general quantity $U(t^k)$, where $t^k=k\Delta t$. The first step of the algorithm consists in updating the macroscopic unknowns n, ρ, u, V, Θ, Υ. We start with the uncoupled relations

$$\frac{1}{\Delta t}(n^{k+1}-n^k) = -\int_{\mathbb{R}^N} v\cdot\nabla_x f^k\,\mathrm{d}v = -\nabla_x\cdot(n^kV^k),$$
$$\frac{1}{\Delta t}(\rho^{k+1}-\rho^k) = -\nabla_x\cdot(\rho^ku^k),$$

which determines the densities n^{k+1} and ρ^{k+1}. Then, the velocities u^{k+1} and V^{k+1} are obtained by solving the system

$$\frac{n^{k+1}V^{k+1}-n^kV^k}{\Delta t} = -\int_{\mathbb{R}^N} v\ v\cdot\nabla_x f^k\,\mathrm{d}v - \eta_P n^k\nabla_x\Phi - \frac{n^{k+1}}{\varepsilon}(V^{k+1}-u^{k+1}),$$
$$\frac{\rho^{k+1}u^{k+1}-\rho^ku^k}{\Delta t} = -\mathrm{Div}_x(\rho^ku^k\otimes u^k+\rho^k\Theta^k) - \eta_F\rho^k\nabla_x\Phi + \frac{\rho_P}{\rho_F}\frac{n^{k+1}}{\varepsilon}(V^{k+1}-u^{k+1}).$$

Note that n^{k+1} has already been determined, and this step reduces to invert N 2×2 linear systems for each component of V^{k+1} and u^{k+1}, which can be inverted *analyti-*

cally. Finally, the temperature Θ and the energy Υ are updated with the system

$$\begin{aligned}
&\frac{1}{\Delta t}(\Upsilon^{k+1}-\Upsilon^k)\\
&=-\int\frac{v^2}{2}\,v\cdot\nabla_x f^k\,\mathrm{d}v-\eta_P n^k V^k\cdot\nabla_x\Phi\\
&\qquad-\frac{1}{\varepsilon}(2\Upsilon^{k+1}-n^{k+1}V^{k+1}\cdot u^{k+1}-Nn^{k+1}\Theta^{k+1}),\\
&\frac{1}{\Delta t}\Big(\frac{\rho^{k+1}|u^{k+1}|^2-\rho^k|u^k|^2}{2}+\frac{\rho^{k+1}\Theta^{k+1}-\rho^k\Theta^k}{\gamma-1}\Big)\\
&=-\mathrm{Div}_x\Big(\Big(\frac{\rho^k|u^k|^2}{2}+\frac{\gamma}{\gamma-1}\rho^k\Theta^k\Big)u^k\Big)-\eta_F\rho^k u^k\cdot\nabla_x\Phi\\
&\qquad+\frac{1}{\varepsilon}\frac{\rho_P}{\rho_F}(2\Upsilon^{k+1}-n^{k+1}V^{k+1}\cdot u^{k+1}-Nn^{k+1}\Theta^{k+1}).
\end{aligned}$$

Since n^{k+1}, u^{k+1}, V^{k+1} are already known, this step reduces to invert a 2×2 linear system for Υ^{k+1} and Θ^{k+1}, which can (again) be done *analytically.* Having these quantities at hand, one can update the Maxwellian, $M^{k+1}(v)=M_{u^{k+1},\Theta^{k+1}}(v)$. The second step updates the particle distribution function by

$$\frac{1}{\Delta t}(f^{k+1}-f^k)=-(v\cdot\nabla_x f^k-\eta_P\nabla_x\Phi\cdot\nabla_v f^k)+\frac{\Theta^{k+1}}{\varepsilon}\mathrm{Div}_v\Big(M^{k+1}\nabla_v\Big(\frac{f^{k+1}}{M^{k+1}}\Big)\Big).$$

Let us postpone for a while the question of inverting the Fokker–Planck operator, and begin with a discussion on space and velocity discretizations.

3.2. The time discretization – second order. We can extend the time discretization to second order. We replace the time discretization $\frac{1}{\Delta t}((\cdot)^{k+1}-(\cdot)^k)$ by a BDF type second order discretization $\frac{1}{2\Delta t}(3(\cdot)^{k+1}-4(\cdot)^k+(\cdot)^{k-1})$. The explicit terms $(\cdot)^k$ are replaced by $(2(\cdot)^k-(\cdot)^{k-1})$. The stiff parts are still formulated implicitly as $(\cdot)^{k+1}$. We now give the algorithm in detail.

Again we update first the macroscopic unknowns n, ρ, u, V, Θ, Υ. We start with

$$\begin{aligned}
\frac{3n^{k+1}-4n^k+n^{k-1}}{2\Delta t}&=-\int_{\mathbb{R}^N}v\cdot\nabla_x(2f^k-f^{k-1})\,\mathrm{d}v=-\nabla_x\cdot(2n^kV^k-n^{k-1}V^{k-1}),\\
\frac{3\rho^{k+1}-4\rho^k+\rho^{k-1}}{2\Delta t}&=-\nabla_x\cdot(2\rho^k u^k-\rho^{k-1}u^{k-1}),
\end{aligned}$$

which determine the densities n^{k+1} and ρ^{k+1}. Then, the velocities u^{k+1} and V^{k+1} are obtained by solving the system

$$\begin{aligned}
&\frac{1}{\Delta 2t}(3n^{k+1}V^{k+1}-4n^kV^k+n^{k-1}V^{k-1})\\
&=-\frac{n^{k+1}}{\varepsilon}(V^{k+1}-u^{k+1})-\int_{\mathbb{R}^N}v\;v\cdot\nabla_x(2f^k-f^{k-1})\,\mathrm{d}v-\eta_P(2n^k-n^{k-1})\nabla_x\Phi,\\
&\frac{1}{\Delta 2t}(3\rho^{k+1}u^{k+1}-4\rho^ku^k+\rho^{k-1}u^{k-1})\\
&=\frac{\rho_P}{\rho_F}\frac{n^{k+1}}{\varepsilon}(V^{k+1}-u^{k+1})-\eta_F(2\rho^k-\rho^{k-1})\nabla_x\Phi\\
&\qquad-\mathrm{Div}_x(2(\rho^ku^k\otimes u^k+\rho^k\Theta^k)-(\rho^{k-1}u^{k-1}\otimes u^{k-1}+\rho^{k-1}\Theta^{k-1})).
\end{aligned}$$

Finally, the temperature Θ and the energy Υ are updated with the system

$$\begin{aligned}
&\frac{1}{\Delta 2t}(3\Upsilon^{k+1}-4\Upsilon^{k}+\Upsilon^{k-1})\\
&=-\int\frac{v^2}{2}\ v\cdot\nabla_x(2f^k-f^{k-1})\,\mathrm{d}v\\
&\quad -\eta_{_P}(2n^kV^k-n^{k-1}V^{k-1})\cdot\nabla_x\Phi-\frac{1}{\varepsilon}(2\Upsilon^{k+1}-n^{k+1}V^{k+1}\cdot u^{k+1}-Nn^{k+1}\Theta^{k+1}),\\
&\frac{1}{\Delta 2t}\Big(\frac{3\rho^{k+1}|u^{k+1}|^2-4\rho^k|u^k|^2+\rho^{k-1}|u^{k-1}|^2}{2}+\frac{3\rho^{k+1}\Theta^{k+1}-4\rho^k\Theta^k+\rho^{k-1}\Theta^{k-1}}{\gamma-1}\Big)\\
&=-\mathrm{Div}_x\left\{2\Big(\frac{\rho^k|u^k|^2}{2}+\frac{\gamma}{\gamma-1}\rho^k\Theta^k\Big)u^k-\Big(\frac{\rho^{k-1}|u^{k-1}|^2}{2}+\frac{\gamma}{\gamma-1}\rho^{k-1}\Theta^{k-1}\Big)u^{k-1}\right\}\\
&\quad -\eta_{_F}(2\rho^ku^k-\rho^{k-1}u^{k-1})\cdot\nabla_x\Phi+\frac{1}{\varepsilon}\frac{\rho_{_P}}{\rho_{_F}}(2\Upsilon^{k+1}-n^{k+1}V^{k+1}\cdot u^{k+1}-Nn^{k+1}\Theta^{k+1}).
\end{aligned}$$

Having these quantities at hand, one can update the Maxwellian, $M^{k+1}(v)=M_{u^{k+1},\Theta^{k+1}}(v)$. The second step updates the particle distribution function by

$$\begin{aligned}
&\frac{1}{2\Delta t}(3f^{k+1}-4f^k+f^{k-1})\\
&=-(v\cdot\nabla_x-\eta_{_P}\nabla_x\Phi\cdot\nabla_v)(2f^k-f^{k-1})+\frac{\Theta^{k+1}}{\varepsilon}\mathrm{Div}_v\Big(M^{k+1}\nabla_v\Big(\frac{f^{k+1}}{M^{k+1}}\Big)\Big).
\end{aligned}$$

In the following sections, we will focus (for simplicity) on the detailed discretization for the first order scheme. However, the second order scheme can be treated in a similar way.

3.3. Space and velocity discretizations. The convection terms can be treated, as in [13], by coupling the upwind scheme in space and the center difference scheme in velocity discretizations, respectively, for the kinetic equation with an anti-diffusive scheme of Finite Volume type [18, 34, 35] for the Euler system. However, we find it convenient to approximate the fluid equations by kinetic schemes. This family of schemes mimics, at the discrete level, the derivation of fluid equations from a kinetic equation through the small mean free path limit; see [15, 16, 17, 44, 45, 46]. It is particularly well-suited to our model since the approximation of the microscopic and macroscopic equations will be based on the same discretization. Consequently, we will obtain for $\varepsilon=0$ a natural kinetic scheme for the system (2.2).

The idea consists in interpreting $\mathscr{U}=(\rho,\rho u,\rho E)$ as the zeroth, first, and second order moments of a particle distribution function $G(t,x,v)$ subject to a strong relaxation. For the monoatomic case, that is for $\gamma=(N+2)/N$ and thus $\rho E=\rho(|u|^2+N\Theta)/2$, the Euler system

$$\partial_t\mathscr{U}+\nabla_x\begin{pmatrix}\rho u\\ \rho u^2+\rho\Theta\\ \rho\big(|u|^2+(N+2)\Theta\big)u/2\end{pmatrix}=\bar{\mathbb{F}}-\eta_{_F}\begin{pmatrix}0\\ \rho\\ \rho u\end{pmatrix}\partial_x\Phi, \tag{3.1}$$

with a force field $\bar{\mathbb{F}}=\int_{\mathbb{R}^N}\mathbb{F}\,\mathrm{d}v$, can be derived from the limit for $\lambda\gg 1$ of the following BGK equation:

$$(\partial_t+v\nabla_x-\eta_{_F}\partial_x\Phi\nabla_v)G=\mathbb{F}+\lambda(\mathscr{M}[G]-G),$$

with

$$\mathscr{M}[G]=\frac{\rho_G}{(2\pi\Theta_G)^{N/2}}\exp\Big(-\frac{|v-u_G|^2}{2\Theta_G}\Big),$$
$$\begin{pmatrix}\rho_G\\ \rho_G u_G\\ \rho_G|u_G|^2+N\rho_G\Theta_G\end{pmatrix}=\int_{\mathbb{R}^N}\begin{pmatrix}1\\ v\\ v^2\end{pmatrix}G\,\mathrm{d}v=\int_{\mathbb{R}^N}\begin{pmatrix}1\\ v\\ v^2\end{pmatrix}\mathscr{M}[G]\,\mathrm{d}v.$$

We refer for instance to [9, 48] for results and comments on the analysis of this small mean free path regime. It leads to the following construction for solving (3.1), which is based on a time splitting of the BGK equation:

- Define $G^\star$ from the transport equation

$$\frac{1}{\Delta t}(G^\star-G^k)+v\cdot\nabla_x G^k-\eta_{_F}\nabla_x\Phi\cdot\nabla_v G^k=\mathbb{F}^{k+1};$$

- Project the solution to the equilibrium state

$$G^{k+1}=\mathscr{M}[G^\star].$$

For describing a more general state law, one needs a coupled system of kinetic equations defined as follows:

$$(\partial_t+v\cdot\nabla_x-\eta_{_F}\nabla_x\Phi\cdot\nabla_v)G_1=\mathbb{F}+\lambda(\mathscr{M}-G_1),$$
$$\partial_t G_2+v\cdot\nabla_x G_2=\lambda(\mathscr{N}-G_2),$$

with $\lambda\gg 1$. A possible definition of $\mathscr{M}$ and $\mathscr{N}$ that generalizes the Maxwellian distribution is

$$\mathscr{M}(v)=\frac{\rho}{(2\pi\Theta)^{N/2}}\exp\Big(-\frac{|v-u|^2}{2\Theta}\Big),$$
$$\mathscr{N}(v)=\frac{2-N(\gamma-1)}{2(\gamma-1)}\frac{\rho\Theta}{(2\pi\Theta)^{N/2}}\exp\Big(-\frac{|v-u|^2}{2\Theta}\Big),$$

where the macroscopic quantities are given by

$$\begin{pmatrix}\rho\\ \rho u\\ \dfrac{\rho|u|^2}{2}+\dfrac{\rho\Theta}{(\gamma-1)}\end{pmatrix}=\int_{\mathbb{R}^N}\begin{pmatrix}G_1\\ vG_1\\ \dfrac{v^2}{2}G_1+G_2\end{pmatrix}\mathrm{d}v=\int_{\mathbb{R}^N}\begin{pmatrix}\mathscr{M}\\ v\mathscr{M}\\ \dfrac{v^2}{2}\mathscr{M}+\mathscr{N}\end{pmatrix}\mathrm{d}v.$$

The scheme for the polytropic Euler system is now constructed as follows:

- Define $G_1^\star$ from the transport equation

$$\frac{1}{\Delta t}(G_1^\star-G_1^k)+v\cdot\nabla_x G_1^k-\eta_{_F}\nabla_x\Phi\cdot\nabla_v G_1^k=\mathbb{F}^{k+1},$$

  and $G_2^\star$ from

$$\frac{1}{\Delta t}(G_2^\star-G_2^k)+v\cdot\nabla_x G_2^k=0;$$

- Project the solution to the equilibrium state

$$G_1^{k+1} = \mathscr{M}, \qquad G_2^{k+1} = \mathscr{N},$$

with macroscopic quantities defined by moments of $G_1^\star$ and $G_2^\star$.

Of course this construction is fictitious since in the implementation of kinetic schemes one only uses the macroscopic variables defined in the physical space, which are obtained by taking moments on the above procedures rather than the variable v or the microscopic quantities G_j. We refer to [15, 44], [45, Sections 1.7–1.10 & Section 8], or [25, Chapter III–Section 7] for a detailed introduction to kinetic schemes. The choice of equilibrium states based on the Maxwellian might look natural in view of the derivation of the Euler system from kinetic equations in the small mean free path regime [9, 48]. In particular, for the monoatomic case it leads to an elegant formula in the scheme for the coupled fluid/particles limit system; see (3.6) below. However, for numerical purposes other definitions of $\mathscr{M}$ and $\mathscr{N}$ are possible. In particular, dealing with compactly supported functions makes stability issues clear; see [44, Theorem 3], [25, Proposition 7.3 & Theorem 7.2], and [45, Sections 1.7–1.10 & Section 8, sp. Theorem 8.3.1]. For instance, for the monoatomic case $\gamma = (N+2)/N$ ($\delta = 0$) one can use the following compactly-supported function:

$$\mathscr{M}[G] = \frac{1}{\mathrm{meas}(B_N)} \; \frac{\rho}{\big((N+2)\Theta\big)^{N/2}} \; \mathbf{1}_{|v-u| \le \sqrt{(N+2)\Theta}}$$

(note that in dimension one, the monoatomic case corresponds to $\gamma = 3$). The numerical fluxes obtained this way coincide with Van Leer's fluxes [25, Example 7.2].

Let us restrict the presentation of the space and velocity discretizations to the one-dimension framework. We consider a meshing of the domain, say $(-L, L)$, with J points separated by the step Δx. The velocity is truncated to the domain $(-V_{\mathrm{Max}}, +V_{\mathrm{Max}})$, discretized with a symmetric set of velocities $(v_1, ..., v_{2M})$, with step Δv. We denote by $f_{j,m}^k$ the numerical approximation of a microscopic quantity $f(k\Delta t, x_j, v_m)$ and denote by

$$\big\langle f \big\rangle_j^k := \frac{\Delta v}{2} \Big(f_{j,1}^k + f_{j,2M}^k + 2 \sum_{m=2}^{2M-1} f_{j,m}^k \Big)$$

the approximation of the velocity average by the trapezoidal rule. This formula is chosen to ensure that the even moments of the odd functions with respect to v vanish; see [13]. For the sake of simplicity, we consider the simplest upwind discretization of the advection operator $v\partial_x$:

$v\partial_x f(k\Delta t, x_j, v_m)$ is approximated by

$$v D_x[f]_{j,m}^k = \frac{1}{2\Delta x} \big((v_m + |v_m|)(f_{j,m}^k - f_{j-1,m}^k) + (v_m - |v_m|)(f_{j+1,m}^k - f_{j,m}^k) \big).$$

More elaborate versions of the kinetic scheme can be used that reach second order accuracy and incorporate a slope limiter to suppress numerical oscillations across shocks, see [25, Section 7.3.4] and [44, Sections 2.2 & 4.2]. For the external force term, we can adopt a centered approximation of the v-derivative which yields (see [13])

$\partial_x \Phi \partial_v f(k\Delta t, x_j, v_m)$ is approximated by

$$v D_x[\Phi]_{j,m}^k \; \frac{1}{v_m} \; D_v[f]_{j,m}^k = v D_x[\Phi]_{j,m}^k \; \frac{1}{v_m} \; \frac{f_{j,m+1}^k - f_{j,m-1}^k}{2\Delta v}.$$

When the amplitude of the potential remains moderate compared to $1/\varepsilon$ it does not affect the stability of the scheme since the velocity diffusion term is treated implicitly in the Fokker–Planck operator. When the external force becomes large, upwinding must be preferred; for instance

$\partial_x\Phi\partial_v f(k\Delta t,x_j,v_m)$ is approximated by

$$\frac{1}{2\Delta v}\Big((\partial_x\Phi_j-|\partial_x\Phi_j|)(f^k_{j,m}-f^k_{j,m-1})+(\partial_x\Phi_j+|\partial_x\Phi_j|)(f^k_{j,m+1}-f^k_{j,m})\Big).$$

REMARK 3.1. In numerical simulation we are applying the following second order finite volume scheme on the external force term (in fact the x derivative term is solved by the same scheme):

$\partial_x\Phi\partial_v f(k\Delta t,x_j,v_m)$ is approximated by

$$\frac{1}{2\Delta v}\Big((\partial_x\Phi_j-|\partial_x\Phi_j|)(F^+_{j,m+1/2}-F^+_{j,m-1/2})+(\partial_x\Phi_j+|\partial_x\Phi_j|)(F^-_{j,m+1/2}-F^-_{j,m-1/2})\Big),$$

with

$$F^+_{j,m+1/2}=f_{j,m}+\sigma_{j,m}\tfrac{f_{j,m+1}-f_{j,m}}{2},$$
$$F^-_{j,m+1/2}=f_{j,m+1}-\sigma_{j,m+1}\tfrac{f_{j,m+1}-f_{j,m}}{2},$$

and

$$\sigma_{j,m}=\phi\left(\frac{f_{j,m}-f_{j,m-1}}{f_{j,m+1}-f_{j,m}}\right),$$

where the limiter function $\phi(\Theta)$ is, for example, the van Leer limiter

$$\phi(\Theta)=\frac{\Theta+|\Theta|}{1+|\Theta|}$$

or the minmod limiter

$$\phi(\Theta)=\max\{0,\min\{1,\Theta\}\}.$$

This discretization imposes a stability constraint, $\frac{|\partial_x\Phi|\Delta t}{\Delta v}\le\frac{1}{2}$, in addition to the constraint due to spatial discretization of $v\partial_x f$.

Finally, given discrete density, velocity, and temperature $(\rho^k_j,u^k_j,\Theta^k_j)$, denote

$$M^k_{j,m}:=\frac{1}{\sqrt{2\pi\Theta^k_j}}\exp\Big(-\frac{|v_m-u^k_j|^2}{2\Theta^k_j}\Big),$$
$$\mathscr{M}^k_{j,m}:=\frac{\rho^k_j}{\sqrt{2\pi\Theta^k_j}}\exp\Big(-\frac{|v_m-u^k_j|^2}{2\Theta^k_j}\Big),$$
$$\mathscr{N}^k_{j,m}:=\frac{2-(\gamma-1)}{2(\gamma-1)}\frac{\rho^k_j\Theta^k_j}{\sqrt{2\pi\Theta^k_j}}\exp\Big(-\frac{|v_m-u^k_j|^2}{2\Theta^k_j}\Big),$$

and $\mathscr{L}f^k_{j,m}$ the corresponding approximation of $L_{u,\Theta}f$ at $(k\Delta t,x_j,v_m)$. The precise form of this approximation will be detailed in the next section. Then the fully discretized form of the algorithm reads as follows:

- Step 1. Updating the macroscopic quantities: Find $(\rho_j^{k+1}, n_j^{k+1}, u^{k+1}, V_j^{k+1}, \Theta_j^{k+1}, \Upsilon_j^{k+1})$ which solve

$$\begin{aligned}
\frac{1}{\Delta t}(n_j^{k+1}-n_j^k) &= -\big\langle vD_x[f]\big\rangle_j^k,\\
\frac{1}{\Delta t}(\rho_j^{k+1}-\rho_j^k) &= -\big\langle vD_x[\mathscr{M}]\big\rangle_j^k,\\
\frac{1}{\Delta t}(n_j^{k+1}V_j^{k+1}-n_j^kV_j^k) &= -\big\langle v\ vD_x[f]\big\rangle_j^k+\eta_{_P}\Big\langle vD_x[\Phi]\ D_v[f]\Big\rangle_j^k\\
&\qquad -\frac{n_j^{k+1}}{\varepsilon}(V_j^{k+1}-u_j^{k+1}),\\
\frac{1}{\Delta t}(\rho_j^{k+1}u_j^{k+1}-\rho_j^ku_j^k) &= -\big\langle v\ vD_x[\mathscr{M}]\big\rangle_j^k+\eta_{_F}\Big\langle vD_x[\Phi]\ D_v[\mathscr{M}]\Big\rangle_j^k\\
&\qquad +\frac{\rho_{_P}}{\rho_{_F}}\frac{n_j^{k+1}}{\varepsilon}(V_j^{k+1}-u_j^{k+1}),\\
\frac{1}{\Delta t}(\Upsilon_j^{k+1}-\Upsilon_j^k) &= -\Big\langle\frac{v^2}{2}vD_x[f]\Big\rangle_j^k+\eta_{_P}\Big\langle vD_x[\Phi]\ \frac{v}{2}D_v[f]\Big\rangle_j^k\\
&\qquad -\frac{1}{\varepsilon}(2\Upsilon_j^{k+1}-n_j^{k+1}V_j^{k+1}\cdot u_j^{k+1}-n_j^{k+1}\Theta_j^{k+1}),\\
\frac{1}{\Delta t}\Big(E_j^{k+1}-E_j^k\Big) &= -\Big\langle\frac{v^2}{2}vD_x[\mathscr{M}]\Big\rangle_j^k-\big\langle vD_x[\mathscr{N}]\big\rangle_j^k\\
&\qquad +\eta_{_F}\Big\langle vD_x[\Phi]\ \frac{v}{2}D_v[\mathscr{M}]\Big\rangle_j^k\\
&\qquad +\frac{1}{\varepsilon}\frac{\rho_{_P}}{\rho_{_F}}(2\Upsilon_j^{k+1}-n_j^{k+1}V_j^{k+1}\cdot u_j^{k+1}-n_j^{k+1}\Theta_j^{k+1}),
\end{aligned}\tag{3.2}$$

  with $E_j^k := \dfrac{|u_j^k|^2}{2}+\dfrac{\Theta_j^k}{\gamma-1}$;

- Step 2. Updating the particle distribution function. The first step allows to define $M_{j,m}^{k+1}$. Then, we define $f_{j,m}^{n+1}$ as the solution of

$$\frac{1}{\Delta t}(f_{j,m}^{k+1}-f_{j,m}^k)=-vD_x[f]_{j,m}^k+\eta_{_P}vD_x[\Phi]_{j,m}^k\frac{1}{v}D_v[f]_{j,m}^k+\frac{1}{\varepsilon}\mathscr{L}f_{j,m}^{k+1}. \tag{3.3}$$

  It requires the inversion of the operator $(1-\frac{\Delta t}{\varepsilon}\mathscr{L})$ that will be discussed in the next subsection. We finish the time step by setting

$$n_j^{k+1}=\big\langle f\big\rangle_j^{k+1},\qquad n_j^{k+1}V_j^{k+1}=\big\langle vf\big\rangle_j^{k+1},\qquad \Upsilon_j^{k+1}=\frac{1}{2}\big\langle v^2f\big\rangle_j^{k+1}.$$

Remark 3.2. For the boundary condition, we apply the specular reflection law for the particles. For the discrete unknown, the law reads

$$f_{0,2M+1-m}^k=f_{1,m}^k,\qquad f_{J+1,m}^k=f_{J,2M+1-m}^k.$$

For the hydrodynamic unknowns, we use the so-called "wall boundary condition" which are imposed through ghost cells

$$\big(\rho_0^k,u_0^k,\Theta_0^k\big)=\big(\rho_1^k,-u_1^k,\Theta_1^k\big),\quad \big(\rho_{J+1}^k,u_{J+1}^k,\Theta_{J+1}^k\big)=\big(\rho_J^k,-u_J^k,\Theta_J^k\big).$$

We refer for instance to [1] for discussion of numerical boundary conditions for kinetic schemes.

REMARK 3.3. In many situations $\partial_x\Phi=\Psi$ has a simple expression. For instance it is merely constant for gravity–driven flows. Then, the external force terms in (3.2) are replaced by $\eta_P n_j^k\Psi_j$, $\eta_P n_j^k V_j^k\Psi_j$, $\eta_F\rho_j^k\Psi_j$, $\eta_F\rho_j^k u_j^k\Psi_j$.

3.4. Treatment of the Fokker-Planck operator. We follow the method introduced in [33]. Given u and Θ, it is convenient to write

$$L_{u,\Theta}f=\Theta\sqrt{M_{u,\Theta}}\ \tilde{L}_{u,\Theta}h,$$

with

$$h=\frac{f}{\sqrt{M_{u,\Theta}}},\qquad \tilde{L}_{u,\Theta}h=\frac{1}{\sqrt{M_{u,\Theta}}}\mathrm{Div}_v\Big(M_{u,\Theta}\nabla_v\Big(\frac{h}{\sqrt{M}_{u,\Theta}}\Big)\Big).$$

The advantage of this change of unknown lies on the symmetry property

$$\int_{\mathbb{R}^N}\tilde{L}_{u,\Theta}h\ g\,\mathrm{d}v=\int_{\mathbb{R}^N}h\ \tilde{L}_{u,\Theta}g\,\mathrm{d}v.$$

Accordingly, we set

$$h_{j,m}=\frac{f_{j,m}^{k+1}}{\sqrt{M_{j,m}^{k+1}}},\qquad \mathscr{L}f_{j,m}^{k+1}=\Theta_j^{k+1}\sqrt{M_{j,m}^{k+1}}\ \tilde{\mathscr{L}}h_{j,m},$$

where the discrete operator $\tilde{\mathscr{L}}$ will be symmetric — allowing the inversion of the implicit term by the effective Conjugate Gradient algorithm. Therefore, Step 2 of the first order scheme in Section 3.1 can be recast as follows:

- Solve the linear system

$$\Big(1-\frac{\Delta t}{\varepsilon}\Theta_j^{k+1}\tilde{\mathscr{L}}\Big)h_{j,m}=\frac{f_{j,m}^k-\Delta t\Big(vD_x[f]_{j,m}^k-\eta_P vD_x[\Phi]_{j,m}^k\frac{1}{v}D_v[f]^k\Big)}{\sqrt{M_{j,m}^{k+1}}};$$

- Set $f_{j,m}^{k+1}=h_{j,m}\sqrt{M_{j,m}^{k+1}}$.

In the one–dimension setting, the discrete operator $\tilde{\mathscr{L}}$ is defined as follows (see [33]):

$$\tilde{\mathscr{L}}h_{j,m}=\frac{1}{\Delta v^2}\left(h_{j,m+1}-\frac{\sqrt{M_{j,m+1}^{k+1}}+\sqrt{M_{j,m-1}^{k+1}}}{\sqrt{M_{j,m}^{k+1}}}h_{j,m}+h_{j,m-1}\right)\tag{3.4}$$

which indeed leads to a symmetric matrix. Observe that $\tilde{\mathscr{L}}\big(\sqrt{M^{k+1}}\big)_{j,m}=0$.

LEMMA 3.4. *Consider the discrete operator* (3.4) *with the Neumann-like conditions*

$$\begin{aligned}\sqrt{M_{j,1}}(h_{j,0}-h_{j,2})+h_{j,1}(\sqrt{M_{j,2}}-\sqrt{M_{j,0}})&=0,\\ \sqrt{M_{j,2M}}(h_{j,2M-1}-h_{j,2M+1})+h_{j,2M}(\sqrt{M_{j,2M+1}}-\sqrt{M_{j,2M-1}})&=0.\end{aligned}\tag{3.5}$$

This operator is mass–conserving in the sense that

$$\left\langle \sqrt{M}\tilde{\mathscr{L}}h\right\rangle = 0,$$

and entropy–decaying in the sense that

$$\left\langle \sqrt{M}\tilde{\mathscr{L}}h\ln\left(h/\sqrt{M}\right)\right\rangle \leq 0.$$

REMARK 3.5. Note that the definition of the ghost points with respect to the velocity variable depends on the discrete integration rule: if the rectangle rule is used then one should replace (3.5) by $\frac{h_{j,0}}{\sqrt{M_{j,0}}} = \frac{h_{j,1}}{\sqrt{M_{j,1}}}$ and $\frac{h_{j,2M+1}}{\sqrt{M_{j,2M+1}}} = \frac{h_{j,2M}}{\sqrt{M_{j,2M}}}$. The definition looks like an approximation of the Neumann–like boundary condition $M\partial_v(\frac{h}{\sqrt{M}}) = 0 = M\partial_v(f/M)$.

Proof. The key argument relies on the observation

$$\begin{aligned}\sqrt{M_m}&\left(h_{m+1} - \frac{\sqrt{M_{m+1}}+\sqrt{M_{m-1}}}{\sqrt{M_m}}h_m + h_{m-1}\right)\\ &= \sqrt{M_{m+1}M_m}\left(\frac{h_{m+1}}{\sqrt{M_{m+1}}} - \frac{h_m}{\sqrt{M_m}}\right) - \sqrt{M_m M_{m-1}}\left(\frac{h_m}{\sqrt{M_m}} - \frac{h_{m-1}}{\sqrt{M_{m-1}}}\right).\end{aligned}$$

The proof is concluded by summation by parts. ∎

3.5. Properties of the scheme. (*Asymptotic Preserving*) We can study the limit of the scheme as ε goes to 0. First, Step 2 forces $f_{j,m}^{k+1}$ to coincide with the discrete Maxwellian $n_j^{k+1}M_{j,m}^{k+1}$. Then, adding the two momentum equations and the two energy equations and replacing f by the Maxwellian in (3.2), we obtain

$$\begin{aligned}&\frac{1}{\Delta t}(n_j^{k+1} - n_j^k)\\ &= -\left\langle vD_x[nM]\right\rangle_j^k,\\ &\frac{1}{\Delta t}(\rho_j^{k+1} - \rho_j^k)\\ &= -\left\langle vD_x[\mathscr{M}]\right\rangle_j^k,\\ &\frac{1}{\Delta t}\left(\left(\rho_j^{k+1} + \frac{\rho_P}{\rho_F}n_j^{k+1}\right)u_j^{k+1} - \left(\rho_j^k + \frac{\rho_P}{\rho_F}n_j^k\right)u_j^k\right)\\ &= -\left\langle v\ vD_x\left[\mathscr{M} + \frac{\rho_P}{\rho_F}nM\right]\right\rangle_j^k + \eta_P\left\langle vD_x[\Phi]\ \frac{1}{v}D_v\left[\eta_F\mathscr{M} + \eta_P\frac{\rho_P}{\rho_F}nM\right]\right\rangle_j^k\\ &\frac{1}{2\Delta t}\left(\frac{\left(\rho_j^{k+1} + \frac{\rho_P}{\rho_F}n_j^{k+1}\right)|u_j^{k+1}|^2 - \left(\rho_j^k + \frac{\rho_P}{\rho_F}n_j^k\right)|u_j^k|^2}{2}\right.\\ &\qquad\left. + \frac{\rho_j^{k+1}\Theta_j^{k+1} - \rho_j^k\Theta_j^k}{\gamma - 1} + \frac{\rho_P}{\rho_F}\frac{n_j^{k+1}\Theta_j^{k+1} - n_j^k\Theta_j^k}{2}\right)\\ &= -\left\langle \frac{v^2}{2}vD_x\left[\mathscr{M} + \frac{\rho_P}{\rho_F}nM\right]\right\rangle_j^k + \left\langle vD_x[\mathscr{N}]\right\rangle_j^k\left\langle vD_x[\Phi]\ \frac{v}{2}D_v\left[\eta_F\mathscr{M} + \eta_F\frac{\rho_P}{\rho_F}nM\right]\right\rangle_j^k.\end{aligned} \tag{3.6}$$

This is exactly a kinetic scheme for the limit system (2.2). Note that this expression simplifies in the monoatomic case when we use the Maxwellian $\rho_j^k M_{j,m}^k$ as distribution $\mathscr{M}_{j,m}^k$.

(*Well-Balance*) It turns out that stationary solutions are defined by

$$f_S(x,v) = Z_P \exp\Big(-\frac{v^2}{2\Theta} - \frac{\eta_P \Phi(x)}{\Theta}\Big),$$
$$\rho_S(x) = Z_F \exp\Big(-\frac{\eta_F \Phi(x)}{\Theta}\Big), \qquad u(x) = 0, \qquad \Theta > 0 \text{ (constant)},$$

with Z_F and Z_P normalizing constants. For instance one can set

$$Z_P = \frac{M_P}{\rho_P (2\pi\Theta)^{N/2}} \Big(\int e^{-\eta_P \Phi(x)/\Theta}\,\mathrm{d}x\Big)^{-1}, \qquad Z_F = \frac{M_F}{\rho_F} \Big(\int e^{-\eta_F \Phi(x)/\Theta}\,\mathrm{d}x\Big)^{-1},$$

where M_P and M_F correspond to the masses of the disperse and the dense phases respectively. The stationary solutions can be expected to be natural candidates for describing the large time behavior of the solutions, with the parameters M_F, M_P, and Θ determined by the conservation relations

$$M_P = \rho_P \int f(0,x,v)\,\mathrm{d}v\,\mathrm{d}x, \qquad M_F = \rho_F \int \rho(0,x)\,\mathrm{d}x,$$

together with

$$\rho_P \int \Big(\frac{v^2}{2} + \eta_P \Phi(x)\Big) f_S(x,v)\,\mathrm{d}v\,\mathrm{d}x + \rho_F \int \Big(\frac{\Theta}{\gamma - 1} + \eta_F \Phi(x)\Big)\rho_S(x)\,\mathrm{d}x = E_0,$$

where E_0 stands for the total energy given by

$$E_0 = \rho_P \iint \Big(\frac{v^2}{2} + \eta_P \Phi(x)\Big) f(0,x,v)\,\mathrm{d}v\,\mathrm{d}x + \rho_F \int \Big(\frac{|u(0,x)|^2}{2} + \frac{\Theta(0,x)}{\gamma - 1} + \eta_F \Phi(x)\Big)\rho(0,x)\,\mathrm{d}x.$$

E_0 can be recast as

$$M_P\big(N\Theta + \mathscr{P}_P(\Theta)\big) + M_F\Big(\frac{\Theta}{\gamma - 1} + \mathscr{P}_F(\Theta)\Big) = E_0, \tag{3.7}$$

where $\mathscr{P}_P$ and $\mathscr{P}_F$ depend on the potential Φ:

$$\mathscr{P}_P = \frac{\int \eta_P \Phi(x) e^{-\eta_P \Phi(x)/\Theta}\,\mathrm{d}x}{\int e^{-\eta_P \Phi(x)/\Theta}\,\mathrm{d}x}, \qquad \mathscr{P}_F = \frac{\int \eta_F \Phi(x) e^{-\eta_F \Phi(x)/\Theta}\,\mathrm{d}x}{\int e^{-\eta_F \Phi(x)/\Theta}\,\mathrm{d}x}.$$

Observe that

$$\frac{\mathrm{d}}{\mathrm{d}\Theta}\mathscr{P}(\Theta) = \frac{1}{\Big(\Theta \int e^{-\eta_P \Phi(x)/\Theta}\,\mathrm{d}x\Big)^2} \times \Big(\int |\eta_P \Phi(x)|^2\, e^{-\eta_P \Phi(x)/\Theta}\,\mathrm{d}x \int e^{-\eta_P \Phi(x)/\Theta}\,\mathrm{d}x - \Big(\int \eta_P \Phi(x) e^{-\eta_P \Phi(x)/\Theta}\,\mathrm{d}x\Big)^2\Big)$$

is non–negative as a consequence of the Cauchy-Schwarz inequality. Therefore (3.7) uniquely defines $\Theta \geq 0$ for any $E_0 \geq 0$. Modulus $\mathscr{O}(\Delta x)$ and $\mathscr{O}(\Delta v)$ errors in the stationary solutions are preserved by the scheme. If the center difference is used for the external force term, the velocity error becomes of order $\mathscr{O}(\Delta v^2)$ and only involves odd terms with respect to v, so that its velocity average vanishes [13].

4. Numerical simulations

We perform numerical simulation in the one dimension framework, bearing in mind the example of gravity driven flows. **We always use the second order scheme described in Section 3.2**. The spacial domain is the slab $[0,1]$, where x is thought of as a "vertical" variable (with $x=0$ corresponding to the bottom and $x=1$ to the top). The velocity variable lies in the truncated domain $v \in [-V_{\mathrm{Max}}, V_{\mathrm{Max}}]$, and for the simulation we set $V_{\mathrm{Max}} = 6$. In our numerical experiments, the units are chosen such that the gravity constant is $g=1$ for the sake of simplicity. The initial particle distribution function has the form

$$f(0,x,v) = \frac{n(0,x)}{\sqrt{2\pi\Theta_P(0,x)}} \exp\left(-\frac{|v-V(0,x)|^2}{2\Theta_P(0,x)}\right). \tag{4.1}$$

Notice that this distribution is not at equilibrium as far as $V(0,x) \neq u(0,x)$, or $\Theta_P(0,x) \neq \Theta(0,x)$, with $u(0,x)$ and $\Theta(0,x)$ the initial velocity and temperature fields of the fluid, respectively. Finally, the numerical parameters are $\Delta t = 0.4\frac{\Delta x}{V_{\mathrm{Max}}}$. This choice guarantees the stability of the simulation.

4.1. Energy conservation and entropy dissipation. To start with, we check the ability of the scheme in preserving mass, energy, and in dissipating entropy, according to (1.6) and (1.7). For the simulation we present, we initially consider a homogeneous fluid at rest:

$$\rho(0,x) = 1, \qquad u(0,x) = 0, \qquad \Theta(0,x) = 1. \tag{4.2}$$

The distribution of particles is given by (4.1) with

$$n(0,x) = 0.5 + \exp(-80(x-0.5)^2), \qquad V(0,x) = 0, \qquad \Theta_P(0,x) = 1. \tag{4.3}$$

We set $\varepsilon = 0.1$ and $\rho_P/\rho_F = 100$ while the adiabatic constant is $\gamma = 1.4$. The results to be discussed do not significantly change when these parameters vary. Although we will not provide a figure here, owing to the treatment of the boundary condition, the total mass of both phases is (numerically) exactly conserved. Figure 4.1(a) shows the time evolution up to the final time $T=10$ of the total energy, which is a discrete version of (1.6). The discrete energy is not exactly conserved, but by varying the mesh size one can observe that the error remains of order $\mathscr{O}(\Delta x^2)$. This discrepancy can be explained by the influence of the boundary terms that remain when performing the discrete integration by parts in the energy balance.

Next we study the evolution of the entropy. The discretized entropy at time t^n is defined by

$$H^n := \rho_F \int_{\mathbb{R}} \rho^n S^n \,\mathrm{d}x + \rho_P \int_{\mathbb{R}}\int_{\mathbb{R}} f^n \ln(f^n)\,\mathrm{d}v\,\mathrm{d}x,$$

where the numerical integration is done by the trapezoidal rule for v and the rectangle rule for x. In Figure 4.1(b) we compare the discrete time derivative $\frac{H^{n+1}-H^n}{\Delta t}$ (solid line) and the dissipation term, which is a discrete analog of the right hand side of (1.7)

(dashed line). More precisely, the discretized dissipation term is computed based on the equivalent form

$$\frac{\mathrm{d}}{\mathrm{d}t}H=-\frac{\rho_P}{\varepsilon}\left(\int_{\mathbb{R}^N}\int_{\mathbb{R}^N}\frac{\Theta}{f}\left|M_{V,\Theta}\nabla_v\frac{f}{M_{V,\Theta}}\right|^2\mathrm{d}v\,\mathrm{d}x+\int_{\mathbb{R}^N}\int_{\mathbb{R}^N}f\frac{|V-u|^2}{\Theta}\,\mathrm{d}v\,\mathrm{d}x\right). \quad (4.4)$$

Their evolutions have the same qualitative features. In particular, it is remarkable that $\frac{H^{n+1}-H^n}{\Delta t}$ remains negative, establishing a numerical evidence of the decay of entropy.

We consider the evolution of the (macroscopic) kinetic energy of the two phases

$$K_F=\rho_F\int_{\mathbb{R}}\rho u^2\,\mathrm{d}x,\qquad K_P=\rho_P\int_{\mathbb{R}}nV^2\,\mathrm{d}x.$$

The numerical simulation shows that both quantities are decaying, with oscillations presenting a very similar shape, which suggests that the solutions are approaching some stationary state. This is confirmed by Figure 4.2 where we compare the solution at time $T=20$ with the stationary solution having the same mass and energy. We take $\rho_P/\rho_F=100$ and $\rho_P/\rho_F=0.5$, which give different monotonicities in the density profile of particles in stationary solution. The agreement is quite good, with discrepancies that can be explained either by a final time not large enough or by the defect in the energy conservation.

We repeat this simulation with $\varepsilon=10^{-5}$. The results, which are shown in Figure 4.3, are quite similar to the $\varepsilon=0.1$ case. The total energy is conserved with an error of $O(\Delta x^2)$. The entropy dissipation is preserved. The kinetic energy decays with a slower rate.

4.2. Influence of the external force. Now we study the influence of the external force. We remind that for the case of gravity–driven flows, we have $\eta_F=1$ and $\eta_P=1-\rho_F/\rho_P$. Therefore the sign of η_P determines whether the movement of particles is gravity dominated (corresponding to the "+" sign), or buoyancy dominated (corresponding to the "−" sign).

At first, we investigate the standard model where ρ_P and ρ_F are constants corresponding to the mass density of the particles and a typical mass density of the fluid, respectively. We vary the ratio ρ_P/ρ_F. The simulation is performed with the uniform initial data (4.2) for the fluid, while the particles are initially at rest, concentrated at the center of the domain:

$$n(0,x)=\mathbf{1}_{[0.3,0.7]}(x),\qquad V(0,x)=0,\qquad \Theta_P(0,x)=1.$$

The numerical profiles of the hydrodynamic unknowns at final time $T=0.4$ are shown in Figure 4.4, with different values of ρ_P/ρ_F. We take $\varepsilon=1$ and $\gamma=1.4$ on the grid $N_x=50$, $N_v=32$.

Since the fluid is only subject to gravity, the fluid always moves downwards and its density near the bottom ($x=0$) is always higher. By contrast, the particle's repartition depends on the relative value of ρ_P/ρ_F compared to 1. The movement of particles is dominated by buoyancy when $\rho_P/\rho_F<1$; Figure 4.4(a) shows that particles concentrate near the top. When ρ_P/ρ_F tends to 1, the gravity balances the buoyancy and the particles move freely. Due to the interaction with the fluid, the downward direction is more prominent in the movement of particles, as shown in Figure 4.4(b).

When we consider heavy particles, i.e. $\rho_P/\rho_F>1$, both phases are dominated by gravity (as in Figure 4.4(c)(d)) and the two densities are higher at the bottom as

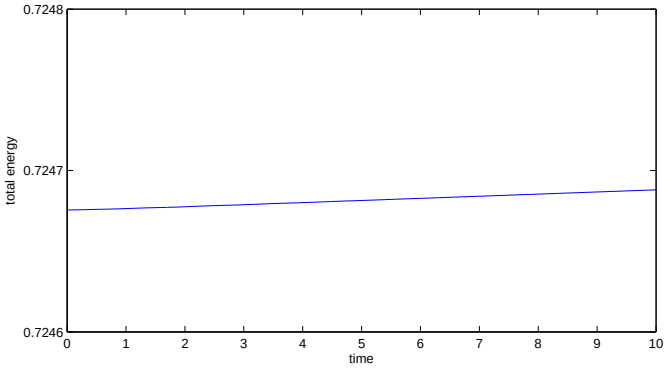

(a) energy conservation

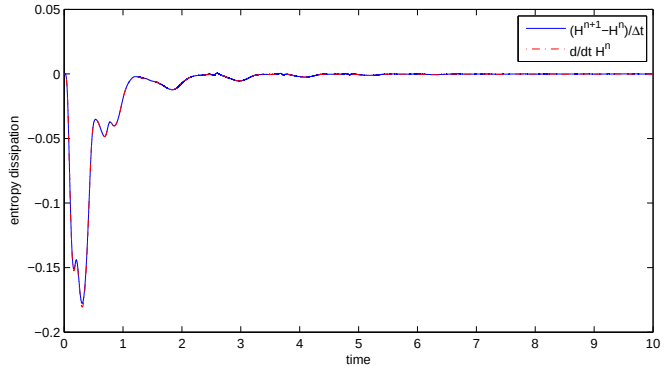

(b) entropy dissipation

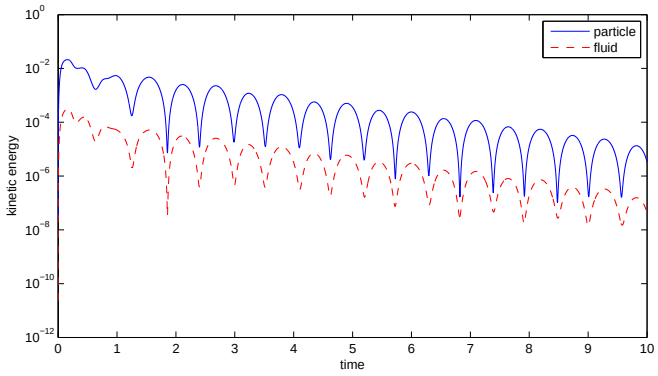

(c) decay of kinetic entropy

FIG. 4.1. *Time evolution of the total energy, total entropy, and the kinetic energy of the two phases, with* $\varepsilon = 0.1$. *Here* $\gamma = 1.4$, $\rho_P/\rho_F = 100$, $N_x = 500$, $N_v = 64$.

time becomes large. It is also worth remarking that particles act like a wall for the fluid, resulting in a clear separation of the domain; this is particularly sensible at the

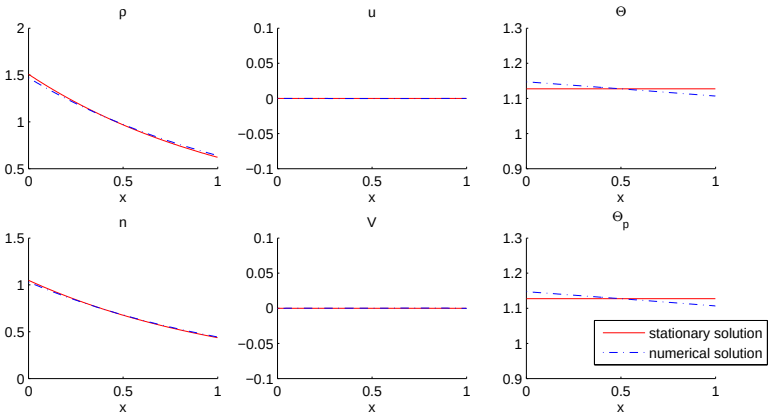

(a) $\rho_P/\rho_F = 100$.

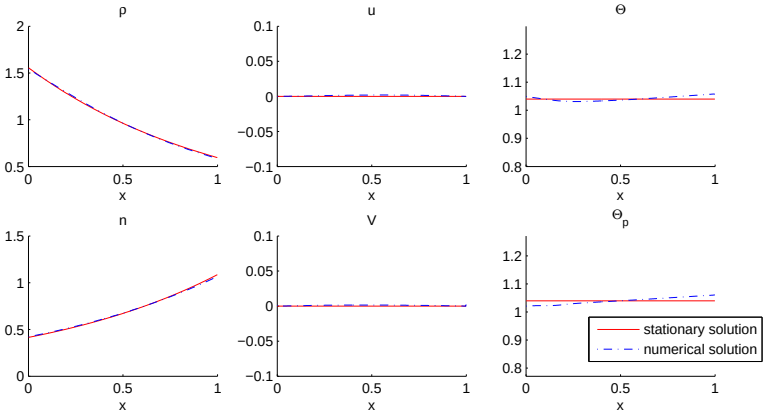

(b) $\rho_P/\rho_F = 0.5$.

FIG. 4.2. *Comparison of the solution (dashed lines) at final time* $T = 20$ *to the stationary solution (solid lines) having the same mass and energy, with different* ρ_P/ρ_F. *Here* $\gamma = 1.4$, $\varepsilon = 0.1$, $N_x = 500$, $N_v = 32$.

beginning of the simulation when a large amount of particles is located at the center of the domain. We also point out that the scheme is able to handle cases with high density ratio, i.e. particles much heavier than the fluid.

It might be questionable to consider a constant reference fluid density in the expression of the buoyancy force because the model varies the fluid density and might create zones of low (resp. high) density. Therefore we perform a couple of simulations by changing ρ_F to $\rho_F \times \rho(t,x)$ in the definition of the buoyancy force. Note however that such a model induces severe technical issues; in particular, in this case the force acting on the particles cannot be derived from a potential and the energy balance becomes unclear. Nevertheless, the simulation brings out some interesting phenomena. We set the initial density of the fluid to be a piecewise constant, so that the motion

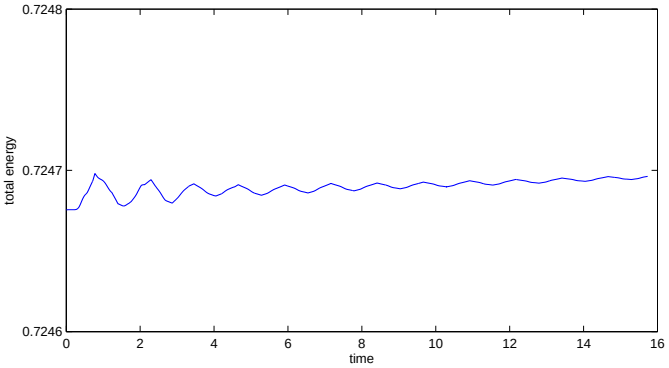

(a) energy conservation

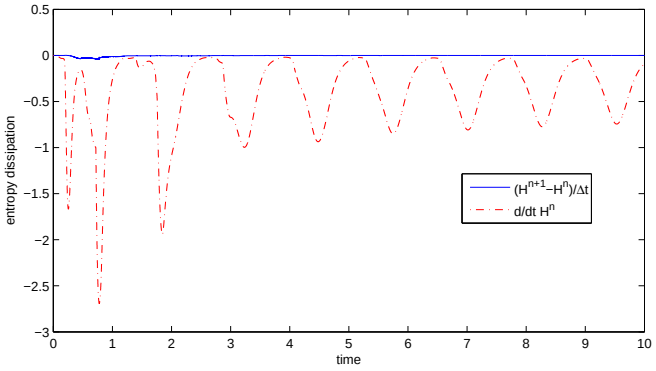

(b) entropy dissipation

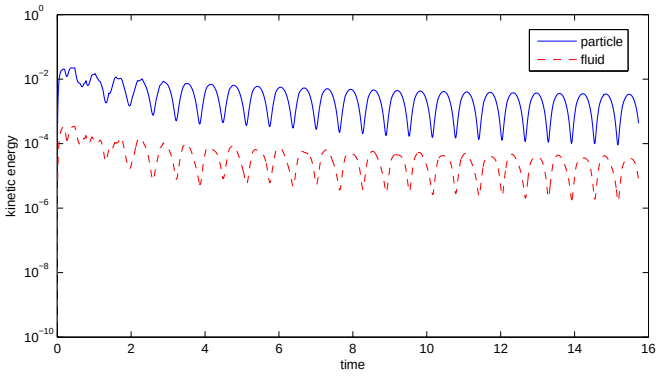

(c) decay of kinetic entropy

FIG. 4.3. *Time evolution of the total energy, total entropy, and the kinetic energy of the two phases, with* $\varepsilon = 10^{-5}$. *Here* $\gamma = 1.4$, $\rho_P/\rho_F = 100$, $N_x = 500$, $N_v = 64$.

of particles are gravity driven in some domains and buoyancy driven in the others:

$$\rho(0,x) = \tfrac{1}{4} + \tfrac{3}{2}\mathbf{1}_{x<1/2}, \qquad u(0,x) = 0, \qquad \Theta(0,x) = 1,$$
$$n(0,x) = 1, \qquad V(0,x) = 0, \qquad \Theta_P(0,x) = 1.$$

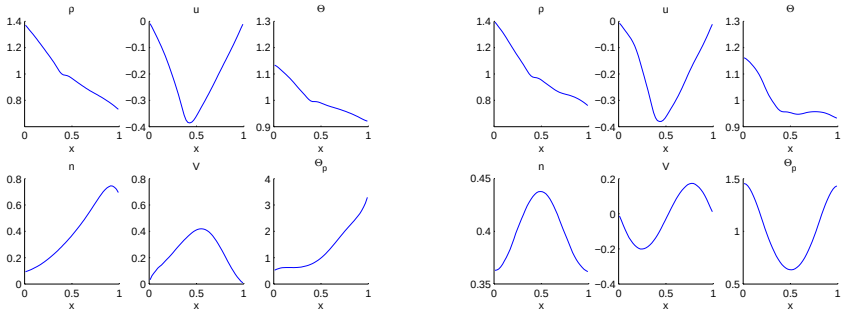

(a) $\frac{\rho_P}{\rho_F}=0.2$ (b) $\frac{\rho_P}{\rho_F}=0.9$

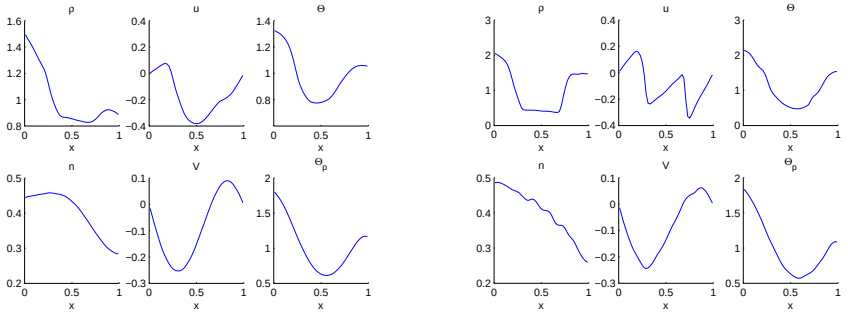

(c) $\frac{\rho_P}{\rho_F}=5$ (d) $\frac{\rho_P}{\rho_F}=100$

FIG. 4.4. *Macroscopic profiles for the fluid (up) and the particles (down) at* $T=0.4$, *with different* ρ_P/ρ_F. *Here* $\gamma=1.4$, $\varepsilon=1$.

We take $\varepsilon=1$, $\gamma=1.4$ on the grid $N_x=50$, $N_v=32$. The profiles of the macroscopic quantities at $T=0.2$ are shown in Figure 4.5, which compares the standard model with a constant reference fluid density (solid lines) and the case that takes density variation into account (dots). The motion of the fluid does not change too much, but the particles move differently, with a clear tendency towards the interface $x=\frac{1}{2}$.

4.3. Asymptotic preserving properties: vanishing Stokes number. In this section we investigate the behavior of the numerical solution as the parameter ε goes to 0. We take $\gamma=1.4$, $\frac{\rho_P}{\rho_F}=100$. The initial data is defined as in (4.2) and (4.1), with

$$n(0,x)=0.5+\exp(-80(x-0.5)^2), \qquad V(0,x)=\exp(-80(x-0.5)^2), \qquad \Theta_P(0,x)=1.$$

We perform simulations with different Stokes number ε, on the same grid $N_x=50$, $N_v=64$. The results at $T=0.3$ are displayed in Figure 4.6. As ε gets smaller, the effects of friction between the two different phases become more and more prominent. The buoyancy effect is dominated by the friction in the case $\varepsilon=10^{-4}$. We observe the (fast) equilibrium of the velocities $u=V$ and temperatures $\Theta=\Theta_P$, as expected from the entropy dissipation and the formal derivation. In order to quantitatively evaluate this effect, we introduce the ℓ^1 distance between the particle distribution f and the

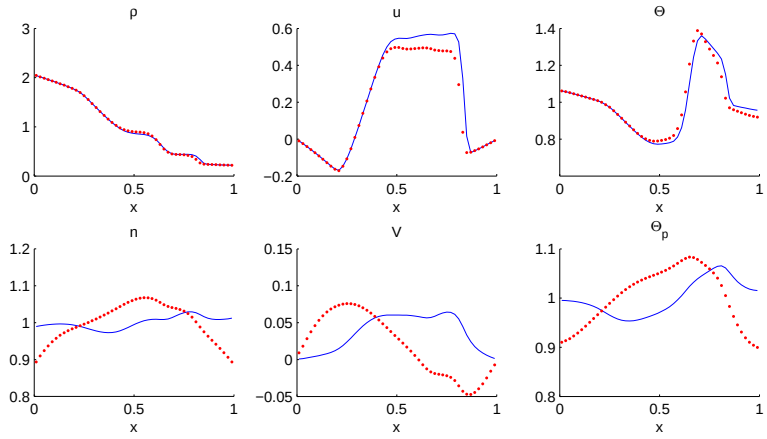

FIG. 4.5. *Macroscopic profiles for the fluid (up) and the particles (down) at* $T=0.2$*: comparison of the model with constant and variable coefficients in the buoyancy force. The solid lines show the results when* ρ_F *is constant, with* $\rho_P/\rho_F=0.9$*. The dots show the results with* x*-dependent* ρ_F*, given by the density of fluid. Here* $\gamma=1.4$*,* $\varepsilon=1$*.*

equilibrium $nM_{u,\Theta}$,

$$\mathrm{dist}(t)=\|f(t,x,v)-nM_{u,\Theta}(t,x,v)\|_1. \tag{4.5}$$

The time evolution of dist(t) for different values of ε is shown in Figure 4.7. As $\varepsilon\to 0$, it shows numerical evidence that $f^k-n^kM_{u^k,\Theta^k}=\mathscr{O}(\varepsilon)$, for $k\geq 1$, which confirms the relaxation effects we conjectured on the formal ground and the AP property of the scheme. In particular, the scheme does not encounter stability difficulties for small ε's; it still works perfectly under stability conditions determined only by the convection terms.

4.4. Temperature dependent viscosity. It makes sense to consider the case where the viscosity μ depends on the temperature of the flows. In particular, Sutherland [51] proposed the formula

$$\mu=\mu_0\left(\frac{\Theta}{\Theta_0}\right)^{3/2}\frac{\Theta_0+S}{\Theta+S},$$

where μ_0 is a reference viscosity, Θ_0 is a reference temperature, and S is an effective temperature, called the Sutherland constant, which is characteristic of the considered fluid. Accordingly, the Fokker–Planck term $\frac{1}{\varepsilon}L_{u,\Theta}f$ is replaced by $\frac{\mu(\Theta)}{\varepsilon}L_{u,\Theta}f$. For the sake of simplicity we take $\mu_0=1$, $T_0=1$, and $S=0.5$. If the stiff term is treated fully implicitly, one is led to a nonlinear system involving $\mu(\Theta^{k+1})$ for determining the hydrodynamic quantities in the first step of the algorithm. A Newton's algorithm is needed, which can impact the performance of the code. We avoid this difficulty by using a semi-implicit formula where the viscosity is set to $\mu(\Theta^k)$ (for the first order scheme) or $\mu(2\Theta^k-\Theta^{k-1})$ (for the second order scheme) instead.

We work with the following initial data:

$$\begin{aligned}&\rho(0,x)=1, \qquad u(0,x)=0, \qquad \Theta(0,x)=0.2+9\ \mathbf{1}_{[0.5,0.6]},\\ &n(0,x)=1, \qquad V(0,x)=0, \qquad \Theta_P(0,x)=1,\end{aligned}$$

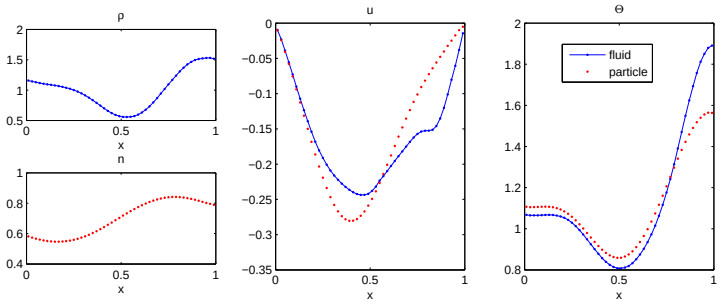

(a) $\varepsilon = 1$

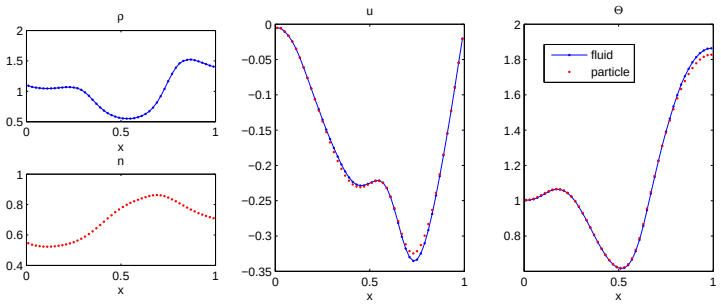

(b) $\varepsilon = 0.1$

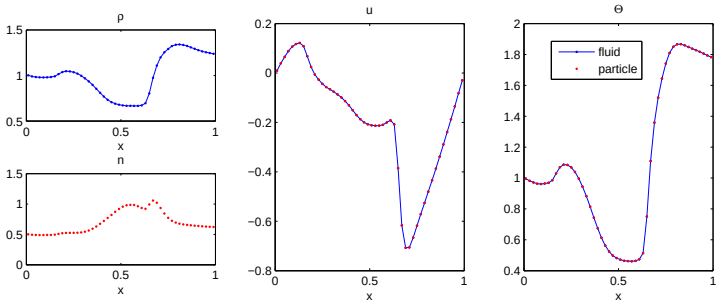

(c) $\varepsilon = 10^{-4}$

FIG. 4.6. *Macroscopic profiles for the fluid (up) and the particles (down) at* $T = 0.3$, *with different* ε. *Here* $\gamma = 1.4$, $\frac{\rho_P}{\rho_F} = 100$.

with $\varepsilon = 1$, $\gamma = 1.4$, and $\rho_P/\rho_F = 5$ on the grid $N_x = 50$, $N_v = 32$. Figure 4.8 shows the profiles of the macroscopic variables at time $T = 0.2$. The dots show the results derived by using the Sutherland viscosity, while the solid lines correspond to the constant viscosity case. The effect of this modification is sensible on the evolution of the temperatures; it seems that the energy exchange is stronger with Sutherland's viscosity. In this case the particles get more energy from the fluid.

4.5. Effects of the state law and different kinetic approximations. We finally check the ability of the scheme to deal with general $\gamma-$state laws. As detailed above, these laws modify the expression of the numerical fluxes for hydrodynamics, as defined by the kinetic scheme. We take $\rho_P/\rho_F = 100$, $\varepsilon = 1$. The initial data are taken

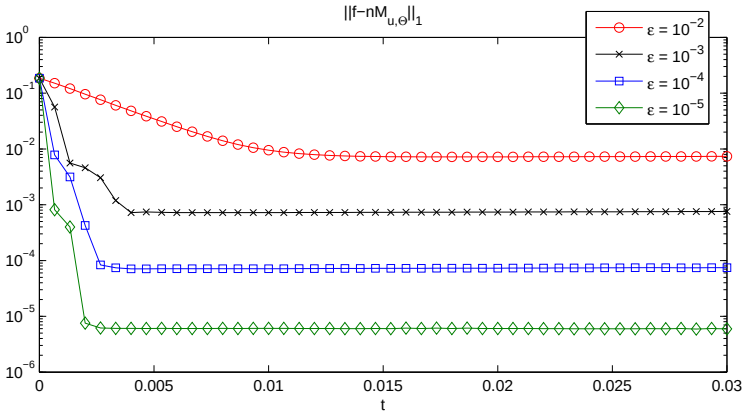

FIG. 4.7. *The L^1 distance between $f(t,x,v)$ and the equilibrium $n(t,x)M_{u(t,x),\Theta(t,x)}(v)$, with different ε. Here $\gamma=1.4$, $\frac{\rho_P}{\rho_F}=100$, $N_x=50$, $N_v=64$.*

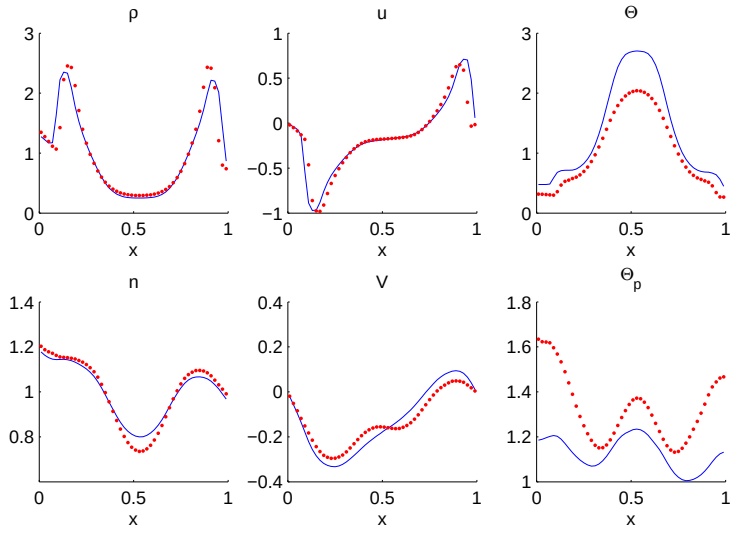

FIG. 4.8. *Macroscopic profiles for the fluid (up) and the particles (down) at $T=0.2$, with constant viscosity (solid lines) and Sutherland's viscosity (dots). Here $\gamma=1.4$, $\varepsilon=1$, $\rho_P/\rho_F=5$.*

as in (4.2) and (4.3). The results at $T=20$ are shown in Figure 4.9. The qualitative behavior of the solutions is not significantly changed. Note in particular that we do not observe the variety of shapes for large time asymptotics as it occurs in the isentropic case (see [12, 13]); all solutions seem to have the same stationary solution as the asymptotic profile. The only difference is in the value of the temperature Θ. This is due to the fact that the energy of fluid differs with different γ, even with the same initial data ρ, u, and Θ.

We also mention that the choice of the equilibrium to be used in the definition

of the kinetic scheme does not influence the simulation, at least in the situations we have tried.

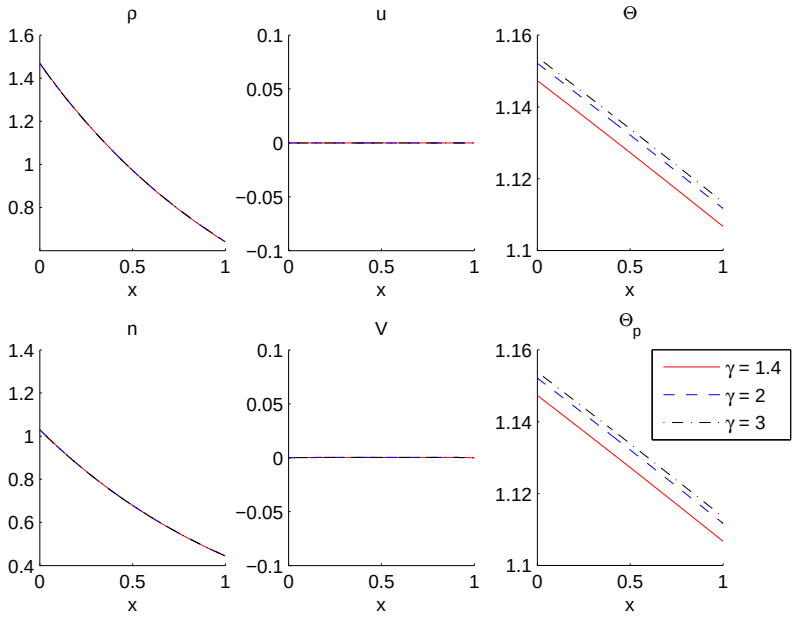

FIG. 4.9. *Macroscopic profiles for the fluid (up) and the particles (down) at* $T=20$, *with different* γ. *Here* $\varepsilon=1$, $\frac{\rho_P}{\rho_F}=100$, $N_x=500$, $N_v=32$.

Conclusion. We have introduced a new numerical scheme for simulating a system coupling the Vlasov–Fokker–Planck Equation to the Euler system through drag force, momentum, and energy exchanges. In particular, the scheme is Asymptotic Preserving in the regime of small Stokes numbers, which drives the system towards a set of purely hydrodynamic equations. The method is based on the implicit treatment of the potentially stiff terms and relies on the possibility of updating the macroscopic unknowns by solving simple linear systems. The use of a kinetic scheme for solving the hydrodynamic equations turns out to be very appropriate because the scheme for the complete problem naturally becomes an extended kinetic scheme for the limit system as the scaling parameter becomes small. Based on numerical evidence, the scheme also exhibits mass conservation, entropy dissipation, and up to mesh dependent error terms, energy conservation, and the well-balanced property. Furthermore, the scheme can easily incorporate relevant generalizations of the basic model like considering general state laws or temperature–dependent viscosities.

Appendix: Scaling issues. Let us detail precisely the scaling issues and the physical meaning of the asymptotic regime we are interested in. To this end, let us go back to the equations written with dimensional quantities. For the sake of concreteness, we restrict the discussion to the three-dimensional case. As usual, $\rho(t,x)$ is the mass density of the fluid and $u(t,x)$ the velocity field. The internal energy is

defined by means of the temperature $\Theta(t,x)$ as follows:

$$\frac{R_s\Theta}{\gamma-1},$$

with $\gamma>1$ the adiabatic constant of the fluid and R_s its specific constant, given by $R_s=R/M_F=k\mathscr{N}/M_F$, with R the perfect gas constant, k the Boltzmann constant, $\mathscr{N}$ the Avogadro number, and M_F the molar mass of the fluid. The particles are described by the quantity $f(t,x,v)$ such that $f(t,x,v)\,\mathrm{d}v\,\mathrm{d}x$ is the probability of finding particles in the domain of the phase space centered at (x,v) with volume $\mathrm{d}v\,\mathrm{d}x$. Accordingly,

$$\frac{4\pi a^3}{3}\int f\,\mathrm{d}v$$

corresponds to the volume fraction occupied by the particles. Multiplying this quantity by ρ_P, the mass density of the particles, we get the mass fraction of the particles. For future use, it is convenient to define the mass of a given particle with radius a:

$$m_P=\frac{4}{3}\pi a^3\rho_P.$$

Particles are subject to the Brownian motion, which induces in the equation a diffusion term with respect to the velocity variable. The diffusion coefficient is given by the Einstein formula [21]

$$\frac{9\mu}{2\rho_P a^2}\ \frac{k\Theta}{m_P},$$

where μ is the dynamic viscosity of the surrounding fluid. The forces acting on the particles split into

- An external force, embodied into the potential Φ and characterized by a certain (real valued) dimensionless coefficient η_P;
- The drag force exerted by the fluid on the particles. Here we assume it is simply given by the Stokes law, and so is a linear expression of the relative velocity

$$6\pi\mu a\ (v-u).$$

The Stokes settling time τ is defined by

$$\frac{1}{\tau}=\frac{6\pi\mu a}{m_P}=\frac{9\mu}{2a^2\rho_P}.$$

We introduce the operator

$$L_{u,\Gamma}f:=\nabla_v\cdot\Big((v-u)f+\Gamma\nabla_v f\Big).$$

Finally, the fluid–particle mixture is described by the following system of PDEs:

$$\begin{cases} \partial_t f + v\cdot\nabla_x f - \eta_P \nabla_x \Phi\cdot\nabla_v f = \dfrac{9\mu}{2\rho_P a^2} L_{u,k\Theta/m_P} f, \\ \partial_t \rho + \nabla_x\cdot(\rho u) = 0, \\ \partial_t(\rho u) + \mathrm{Div}_x\cdot(\rho u\otimes u) + \nabla_x(R_s\rho\Theta) = 6\pi\mu a\displaystyle\int v L_{u,k\Theta/m_P} f\,\mathrm{d}v \\ \qquad\qquad -\eta_F\rho\nabla_x\Phi, \\ \partial_t\Big(\rho\Big(\dfrac{u^2}{2}+\dfrac{R_s\Theta}{\gamma-1}\Big)\Big) + \nabla_x\cdot\Big(\rho u\Big(\dfrac{u^2}{2}+\dfrac{\gamma R_s\Theta}{\gamma-1}\Big)\Big) = 6\pi\mu a\displaystyle\int \frac{v^2}{2} L_{u,k\Theta/m_P} f\,\mathrm{d}v \\ \qquad\qquad -\eta_F\rho u\nabla_x\Phi. \end{cases} \tag{A.1}$$

We are going to write (A.1) in dimensionless form. To this end, we introduce time and length scales of observation, denoted by T and L respectively. Using a typical mass density ρ_F for the fluid, a typical velocity U, and a typical temperature $\bar\Theta$ of the flow, the dimensionless variables and unknowns can be defined as follows:

$$\begin{aligned} t' &= t/\mathrm{T}, & x' &= x/\mathrm{L}, \\ \rho'(t',x') &= \frac{\rho(t,x)}{\rho_F}, & u'(t',x') &= \frac{u(t,x)}{\mathrm{U}}, \\ \Theta'(t',x') &= \frac{\Theta(t,x)}{\bar\Theta}. \end{aligned}$$

For the particles, set

$$\mathrm{V} := \sqrt{\frac{3k\bar\Theta}{4\pi a^3\rho_F}},$$

the thermal velocity and consider a typical volume fraction $0<\bar\phi<1$. Then, define the dimensionless particle distribution function as follows

$$f'(t',x',v') = \frac{4\pi a^3\mathrm{V}^3}{3\bar\phi}\ f(t,x,v).$$

(Therefore $\bar\phi\mathrm{L}^3$ gives the volume occupied by the particles in the reference volume.) Finally, one needs a dimensionless version of the external potential, given by

$$\Phi'(x') = \frac{\Phi(x)}{\bar\Phi}.$$

Using these definitions, (A.1) becomes

$$
\begin{aligned}
&\partial_{t'} f' + \frac{\mathrm{VT}}{\mathrm{L}} v' \cdot \nabla_{x'} f' - \frac{\bar{\Phi}\mathrm{T}}{\mathrm{LV}} \eta_P \nabla_{x'} \Phi' \cdot \nabla_{v'} f' \\
&= \frac{\mathrm{T}}{\tau} L_{\mathrm{U}u'/\mathrm{V},\Theta'} f', \\
&\partial_{t'} \rho' + \frac{\mathrm{UT}}{\mathrm{L}} \nabla_{x'} \cdot (\rho' u') \\
&= 0, \\
&\partial_{t'} (\rho' u') + \frac{\mathrm{UT}}{\mathrm{L}} \mathrm{Div}_{x'} \cdot (\rho' u' \otimes u') + R_s \bar{\Theta} \frac{\mathrm{T}}{\mathrm{LU}} \nabla_{x'} (\rho' \Theta') \\
&= \bar{\phi} \frac{\rho_P}{\rho_F} \frac{\mathrm{T}}{\tau} \frac{\mathrm{V}}{\mathrm{U}} \int v' L_{\mathrm{U}u'/\mathrm{V},\Theta'} f' \, \mathrm{d}v' - \frac{\mathrm{T}\bar{\Phi}}{\mathrm{UL}} \eta_F \rho' \nabla_{x'} \Phi', \\
&\partial_{t'} \Big(\rho' \Big(\frac{|u'|^2}{2} + \frac{R_s \bar{\Theta}}{\mathrm{U}^2} \frac{\Theta'}{\gamma - 1} \Big) \Big) + \frac{\mathrm{TU}}{\mathrm{L}} \nabla_{x'} \cdot \Big(\rho' u' \Big(\frac{|u'|^2}{2} + \frac{R_s \bar{\Theta}}{\mathrm{U}^2} \frac{\gamma \Theta'}{\gamma - 1} \Big) \Big) \\
&= \bar{\phi} \frac{\rho_P}{\rho_F} \frac{\mathrm{T}}{\tau} \Big(\frac{\mathrm{V}}{\mathrm{U}} \Big)^2 \int \frac{|v'|^2}{2} L_{\mathrm{U}u/\mathrm{V},\Theta'} f' \, \mathrm{d}v' - \frac{\mathrm{T}\bar{\Phi}}{\mathrm{UL}} \eta_F \rho' u' \nabla_{x'} \Phi'.
\end{aligned}
\tag{A.2}
$$

We realize that the system is driven by the following set of dimensionless parameters:

- The ratio of the typical velocity and the thermal velocity over the reference velocity L/T:

$$\mathrm{U}\frac{\mathrm{T}}{\mathrm{L}}, \qquad \mathrm{V}\frac{\mathrm{T}}{\mathrm{L}};$$

- The ratio of the Stokes settling time $\tau = \frac{2\rho_F a^2}{9\mu}$, which characterizes the drag effects, over the time unit

$$\varepsilon = \frac{\tau}{\mathrm{T}};$$

- A coefficient characterizing the strength of the acceleration induced by the external potential $\frac{\bar{\Phi}\mathrm{T}^2}{\mathrm{L}^2}$;
- The mass ratio $\frac{\mathscr{N}}{M_F} \frac{4\pi a^3 \rho_P}{3}$, which appears in the formula

$$\frac{R_s \bar{\Theta}}{\mathrm{U}^2} = \Big(\frac{\mathrm{V}}{\mathrm{U}} \Big)^2 \frac{R_s}{3} \frac{4\pi a^3 \rho_P}{k},$$

  bearing in mind $R_s = k\mathscr{N}/M_F$.

The regime we are interested is based on the following assumptions:

a) The ratios $\frac{\mathrm{UT}}{\mathrm{L}}$, $\frac{\mathrm{VT}}{\mathrm{L}}$, $\frac{R_s\bar{\Theta}}{\mathrm{U}^2}$, $\frac{\bar{\Phi}\mathrm{T}^2}{\mathrm{L}^2}$, $\bar{\phi}\frac{\rho_P}{\rho_F}$ are supposed to be of the same order of magnitude;

b) The Stokes settling time is small compared to the time of observation; $0 < \varepsilon \ll 1$ is much smaller than the other parameters within the system.

For the sake of simplicity, we have simply set to unity the parameters defined by a), but keeping $\frac{\rho_P}{\rho_F}$ as a relevant free parameter, and we consider the regime where ε goes to 0.

The modeling can be motivated by the formation of soot during certain combustion processes. Soot is made of pure carbon clusters, with most in the sub-micrometer range of 100 nanometers referred to as ultrafine particles ($PM_{0.1}$ in related nomenclatura). Such very tiny particles constitute the most important aerosol species in the air (up to 80 % of the urban aerosol) and they are a major concern for respiratory exposure and health because of their ability to penetrate deep within the lung. Diesel exhaust is a common example of a source of such particles [47]. Another example comes from the composition of volcanic plumes, a typical signature affecting both the concentration of coarse (larger than $1\mu m$) and ultrafine particles [49]. In a different context, involving a different range of velocity and temperature, we can mention the formation of ocean sprays, which has been reported to play a role in the dynamics of cyclones [37]. Therefore, let us motivate the scaling with the following set of parameters: for soot formation we consider ultrafine particles with typical size $a = 5 \times 10^{-8}$ m. and with mass density $\rho_P = 10^3$ kg m^{-3}. The typical temperature of the device is $\bar{\Theta} = 1000$ K. Then, considering the physical properties of air, we get $M_F = 2.9 \times 10^{-2}$ kg mol^{-1}, $\rho_F = 3.5 \times 10^{-1}$ kg m^{-3}, and for the viscosity $\mu = 4.15 \times 10^{-5}$ kg m^{-1}s^{-1}. A relevant velocity is given by $\mathrm{U} = 100$ m s^{-1}; hence, we choose $\mathrm{L} = 10^{-1}$ m and $\mathrm{T} = 10^{-3}$ s (the use of the compressible Euler equations makes sense due to the fact that the Mach number is of order unity and the Reynolds number is of order 7×10^4 and the particulate Reynolds number is of order 4×10^{-2}, so that the Stokes law can be applied). The relaxation time is $\frac{2}{9}\rho_P \frac{a^2}{\mu} = 1.3 \times 10^{-8}$ s, which is indeed small compared to T. The thermal velocity satisfies $\mathrm{V}^2 = 2.6 \times 10^{-2}$ m s^{-1}. Note that it produces a quite small value of the ratio V/U, of order 10^{-3}. By the way, this is also the order of magnitude of the acceleration term $\bar{\Phi}\mathrm{T}^2/\mathrm{L}^2$ due to gravity. Finally, we obtain $\frac{\mathcal{N}}{M_F} \frac{4\pi a^3 \rho_P}{3} = 10^7$ kg, so that $R_s \bar{\Theta}/\mathrm{U}^2 = 26$. We will further investigate such realistic flows by using our numerical methods elsewhere.

Acknowledgment.

This work started with a visit of Thierry Goudon to the Mathematics Department of UW-Madison. Thanks are addressed for the warm hospitality of the Department.

REFERENCES

[1] D. Aregba-Driollet and V. Milisik, *Kinetic approximation of a boundary value problem for conservation laws*, Numer. Math., 97, 595–633, 2004.

[2] C. Baranger, L. Boudin, P.E. Jabin, and S. Mancini, *A modeling of biospray for the upper airways*, ESAIM: Proc., 14, 41–47, 2005.

[3] C. Baranger and L. Desvillettes, *Coupling Euler and Vlasov equations in the context of sprays: Local smooth solutions*, J. Hyp. Diff. Equ., 3(1), 1–26, 2006.

[4] S. Berres, R. Bürger, and E.M. Tory, *Mathematical model and numerical simulation of the liquid fluidization of polydisperse solid particle mixtures*, Comput. Visual Sci., 6, 67–74, 2004.

[5] L. Boudin, B. Boutin, B. Fornet, T. Goudon, P. Lafitte, F. Lagoutière, and B. Merlet, *Fluid-particles flows: A thin spray model with energy exchanges*, ESAIM: Proc., 28, 195–210, 2009.

[6] L. Boudin, L. Desvillettes, C. Grandmont, and A. Moussa, *Global existence of solutions for the coupled Vlasov and Navier-Stokes equations*, Diff. Int. Equ., 22, 1247–1271, 2009.

[7] B. Boutin and P. Lafitte, *Splitting schemes for fluid-particles flows with energy exchanges*, Work in progress.

[8] R. Bürger, W.L. Wendland, and F. Concha, *Model equations for gravitational sedimentation-consolidation processes*, Z. Angew. Math. Mech., 80(2), 79–92, 2000.

[9] R. Caflisch, *The fluid dynamic limit of the nonlinear Boltzmann equation*, Commun. Pure Appl. Math., 33(5), 651–666, 1980.

[10] R. Caflisch and G. Papanicolaou, *Dynamic theory of suspensions with Brownian effects*, SIAM J. Appl. Math., 43, 885–906, 1983.
[11] J.A. Carrillo, R. Duan, and A. Moussa, *Global classical solutions close to equilibrium to the Vlasov-Euler-Fokker-Planck system*, Kin. Rel. Models, 4, 227–258, 2011.
[12] J.A. Carrillo and T. Goudon, *Stability and asymptotics analysis of a fluid-particles interaction model*, Commun. PDE, 31, 1349–1379, 2006.
[13] J.A. Carrillo, T. Goudon, and P. Lafitte, *Simulation of fluid & particles flows: Asymptotic preserving schemes for bubbling and flowing regimes*, J. Comput. Phys., 227(16), 7929–7951, 2008.
[14] J.A. Carrillo, T. Karpery, and K. Trivisa, *On the dynamics of a fluid-particle interaction model: The bubbling regime*, Nonlin. Anal. TMA, 74, 2778–2801, 2011.
[15] F. Coron and B. Perthame, *Numerical passage from kinetic to fluid equations*, SIAM J. Numer. Anal., 28, 26–42, 1991.
[16] S.M. Deshpande, *Kinetic theory based new upwind methods for inviscid compressible flows*, in AIAA 24th Aerospace Science Meeting, Nevada, USA, Jan, 6-9, 86-0275, 1986.
[17] S.M. Deshpande, *On the Maxwellian distribution, symmetric form and entropy conservation for the Euler equations*, Technical report, NASA Langley Research Centre, Hampton, VA, NASA TP2613, 1986.
[18] B. Després and F. Lagoutière, *Contact discontinuity capturing schemes for linear advection and compressible gas dynamics*, J. Sci. Comput., 16(4), 479–524, 2002.
[19] L. Desvillettes, *Some new results of existence for the theory of sprays*, 2010. `http://www.newton.ac.uk/programmes/KIT/seminars/090710001.html`. Workshop "Fluid-Kinetic Modelling in Biology, Physics and Engineering", Isaac Newton Institute for Mathematical Sciences, Programme on PDEs in Kinetic Theories.
[20] A. Einstein, *On the motion of small particles suspended in liquids at rest required by the molecular-kinetic theory of heat*, Ann. Physik, 17, 549–560, 1905.
[21] A. Einstein, *Eine neue bestimmung der molekü ldimensionen*, Ann. Physik, 19, 289–306, 1906. Doctoral dissertation, Zurich, 1905.
[22] T. Elperin, N. Kleeorin, M.A. Liberman, V.S. L'vov, A. Pomyalov, and I. Rogachevskii, *Clustering of fuel droplets and quality of spray in Diesel engines*, 2003. `http://arxiv.org/nlin.CD/0305017v1`.
[23] G. Falkovich, A. Fouxon, and M.G. Stepanov, *Acceleration of rain initiation by cloud turbulence*, Nature, 219, 151–154, 2002.
[24] F. Filbet and S. Jin, *A class of asymptotic–preserving schemes for kinetic equations and related problems with stiff sources*, J. Comput. Phys., 229(20), 7625–7648, 2010.
[25] E. Godlewski and P.A. Raviart, *Numerical Approximation of Hyperbolic Systems of Conservation Laws*, Appl. Math. Sci., Springer, 118, 1996.
[26] T. Goudon, P.E. Jabin, and A. Vasseur, *Hydrodynamic limit for the Vlasov-Navier-Stokes equations. I. Light particles regime*, Indiana Univ. Math. J., 53(6), 1495–1515, 2004.
[27] T. Goudon, P.E. Jabin, and A. Vasseur, *Hydrodynamic limit for the Vlasov-Navier-Stokes equations. II. Fine particles regime*, Indiana Univ. Math. J., 53(6), 1517–1536, 2004.
[28] T. Goudon, A. Moussa, L. He, and P. Zhang, *The Navier–Stokes–Vlasov–Fokker–Planck system near equilibrium*, SIAM J. Math. Anal., 42(5), 2177–2202, 2010.
[29] K. Hamdache, *Global existence and large time behaviour of solutions for the Vlasov-Stokes equations*, Japan J. Indust. Appl. Math., 15, 51–74, 1998.
[30] M. Ishii and T. Hibiki, *Thermo–Fluid Dynamics of Two–Phase Flows*, Springer, 2nd ed, 2011.
[31] S. Jin, *Efficient asymptotic–preserving (AP) schemes for some multiscale kinetic equations*, SIAM J. Sci. Comput., 21(2), 441–454, 1999.
[32] S. Jin, *Asymptotic preserving (AP) schemes for multiscale kinetic and hyperbolic equations: A review*, Lecture Notes for Summer School on "Methods and Models of Kinetic Theory" (M&MKT), Porto Ercole (Grosseto, Italy), Rivista di Matematica della UniversitÃ di Parma, to appear, June 2010.
[33] S. Jin and B. Yan, *A class of asymmptotic-preserving schemes for the Fokker-Planck-Landau equation*, J. Comput. Phys., 230, 6420–6437, 2011.
[34] F. Lagoutière, *A non-dissipative entropic scheme for convex scalar equations via discontinuous cell-reconstruction*, C.R. Math. Acad. Sci. Paris, 338(7), 549–554, 2004.
[35] F. Lagoutière, *Non-dissipative entropy satisfying discontinuous reconstruction schemes for hyperbolic conservation laws*, Technical report, Univ. Paris–Sud, 2010.
[36] G. Lavergne, *Modélisation de l'écoulement multiphasique dans le propulseur à poudre P230 d'Ariane 5*, 2004. Lecture Notes of the School of the Groupement Français de Combustion, Ile d'Oléron.
[37] J. Lighthill, *Ocean spray and the thermodynamics of tropical cyclones*, J. Eng. Math., 35,

11–42, 1999.
[38] J. Mathiaud, *Etude de Systèmes de Type Gaz-Particules*, PhD thesis, ENS Cachan, 2006.
[39] A. Mellet and A. Vasseur, *Global weak solutions for a Vlasov-Fokker-Planck/Navier-Stokes system of equations*, Math. Mod. Meth. Appl. Sci., 17(7), 1039–1063, 2007.
[40] A. Mellet and A. Vasseur, *Asymptotic analysis for a Vlasov–Fokker–Planck/compressible Navier–Stokes system of equations*, Commun. Math. Phys., 281(3), 573–596, 2008.
[41] A. Moussa, *Etude Mathématique et Numérique du Transport d'Aérosols dans le Poumon Humain*, PhD thesis, ENS Cachan, 2009.
[42] P.J. O'Rourke, *Collective Drop Effects on Vaporizing Liquid Sprays*, PhD thesis, Princeton Univ., 1981. Available as Technical Report #87545 Los Alamos National Laboratory.
[43] M. Pelanti and R. LeVeque, *High resolution finite volume schemes for dusty gas jets and plumes*, SIAM J. Sci. Comput., 28(4), 1335–1360, 2006.
[44] B. Perthame, *Second order Boltzmann schemes for compressible Euler equations in one and two space dimension*, SIAM J. Numer. Anal., 29(1), 1–19, 1992.
[45] B. Perthame, *Kinetic Formulation of Conservation Laws*, Oxford Lecture Series in Math. and its Appl. Oxford University Press, 2003.
[46] D.I. Pullin, *Direct simulation methods for compressible gas flow*, J. Comput. Phys., 34, 231–244, 1980.
[47] L. Rubino, R.I. Crane, J.S. Shrimpton, and C. Arcoumanis, *An electrostatic trap for control of ultrafine particle emissions from gasoline-engined vehicles*, Proc. IMechE. Part D: J. Automobile Engineering, 219, 535–546, 2005.
[48] L. Saint-Raymond, *Hydrodynamic Limits of the Boltzmann Equation*, Lecture Notes in Math., Springer, 1971, 2009.
[49] K. Schäfer, et al., *Influences of the 2010 Eyjafjallajökull volcanic plume on air quality in the northern alpine region*, Atmos. Chem. Phys. Discuss., 9083–9132, 2011.
[50] B. Sportisse, *Modélisation et Simulation de la Pollution Atmosphérique*, PhD thesis, Université Pierre et Marie Curie, 2007. Habilitation à Diriger les Recherches, Sciences de l'Univers.
[51] W. Sutherland, *The viscosity of gases and molecular force*, Philosophical Magazine, S., 5(36), 507–531, 1893.
[52] I. Vinkovic, *Dispersion et Mélange Turbulents de Particules Solides et de Gouttelettes par une Simulation des Grandes Échelles et une Modélisation Stochastique Lagrangienne. Application à la Pollution de l'Atmosphère*, PhD thesis, Ecole Centrale de Lyon, 2005.
[53] F.A. Williams, *Combustion Theory*, Benjamin Cummings Publ., 2nd ed., 1985.